Supporting Information

Stereoregular Functionalized Polysaccharides via Cationic Ring-Opening Polymerization of Biomass-derived Levoglucosan

Mayuri K. Porwal[a], Yernaidu Reddi[b†], Derek J. Saxon[b†], Christopher J. Cramer[b,c], Christopher J. Ellison[a]*, Theresa M. Reineke[b]*

[a] Department of Chemical Engineering and Materials Science, University of Minnesota, Minneapolis, Minnesota 55455, United States

[b] Department of Chemistry, University of Minnesota, Minneapolis, Minnesota 55455, United States

[†]Co-second authors

[c]Underwriters Laboratories Inc., 333 Pfingsten Rd., Northbrook, Illinois 60620, United States

*Corresponding authors

Email: cellison@umn.edu, treineke@umn.edu

Table of Contents

1. General Experimental Protocols

1.1 Materials

Levoglucosan was purchased from Biosynth Carbosynth. 1,6-Anhydro-2,3,4-tri-O-benzyl-β-D-glucopyranose was obtained from Synthose Inc. Anhydrous dichloromethane (CH_2Cl_2, ≥ 99.8%) was purchased from Sigma and used without further purification for polymerizations. MeCN purchased from Fisher was dried over CaH_2 for 3 days, followed by three freeze–pump–thaw cycles, and vacuum transferred before use. Photoinitiator Omnirad 2100 (mixture of 90−95% ethyl(2,4,6-trimethylbenzoyl)phenylphosphinate and 5−10% phenylbis(2,4,6-trimethylbenzoyl)phosphine oxide) was generously provided by IGM Resins. Dextran (number average molecular weight (M_n of 18700 Da) was purchased from Biosynth Carbosynth. Bismuth(III) subsalicylate (99.9% trace metals basis, catalog # 480789), diphenyl phosphoric acid (99%, catalog # 850608), boron trifluoride diethyl etherate (catalog # 175501), methyl trifluoromethanesulfonate (≥98%, catalog # 164283), scandium(III) triflate (99%, catalog # 418218), iron(III) trifluoromethanesulfonate (90%, catalog # 708801), zinc trifluoromethanesulfonate (98%, catalog # 290068), and aluminum isopropoxide (≥98%, catalog # 220418) were purchased from Sigma Aldrich. Yttrium(III) Trifluoromethanesulfonate (≥98%, catalog # T19215G), lanthanum(III) trifluoromethanesulfonate (99%, catalog # AC343910010), aluminum trifluoromethanesulfonate (99%, catalog # AAB2078506), and titanium(IV) isopropoxide (≥98%, catalog # AC194700050) were purchased from Fisher Scientific. Bismuth(III) trifluoromethanesulfonate (99%, catalog # L19687) was purchased from Alfa Aesar. All solid polymerization catalysts were dried under vacuum for 24 h before use. All other reagents and solvents were purchased from commercial sources and used without additional purification.

1.2 Characterization

Nuclear Magnetic Resonance (NMR): A Bruker Avance III HD 400 spectrometer at the University of Minnesota Twin Cities was used to obtain all ^{1}H and ^{13}C NMR spectrums except for the ^{1}H NMR spectrum of poly(4). For better resolution the ^{1}H NMR spectrum of poly(4) was obtained on the Bruker Avance III 500 MHz spectrometer at the University of Minnesota Twin Cities. ^{1}H NMR spectra were referenced to residual solvent shifts of $CHCl_3$ = 7.26 ppm or CH_3OH = 3.31 ppm, and ^{13}C NMR spectra were referenced to residual solvent shifts of $CHCl_3$ = 77.16 ppm. All NMR spectra were analyzed using MestReNova.

Mass Spectrometry: High-resolution mass spectra (HRMS) of synthesized monomer was collected on a Bruker BioTOF II (ESI-TOF) instrument in electrospray ionization (ESI) mode using PPG as an internal calibrant/standard on an Agilent 7200 GC/QTOF instrument. The sample was dissolved in methanol.

Glovebox: All polymerizations were carried out under nitrogen atmosphere in an MBraun Labmaster glovebox.

Size Exclusion Chromatography (SEC):

Molecular weight (M_n and M_w) and dispersity (M_w/M_n) of **poly(2)**, **poly(3)**, and **poly(4)** were determined in DMF containing 0.05M LiBr at a flow rate of 1 mL per minute using an Agilent Infinity 1260 HPLC. The SEC was equipped with a Wyatt DAWN Heleos II multiangle laser light scattering detector (3 angles from 10° to 180°) and a Wyatt OPTILAB T-rEX refractive index detector. dn/dc was calculated from the refractive index signal using a known sample concentration and assuming 100% mass recovery.

M_n, M_w , and M_w/M_n of **poly(5)** was determined in THF with a flow rate of 1 mL per minute on an Agilent Infinity 1260 HPLC with Waters Styragel (HR6, HR5, and HR1) columns connected to a

Wyatt DAWN Heleos II multiangle laser light scattering detector (18 angles from 10° to 180°) and a Wyatt OPTILAB T-rEX refractive index detector. dn/dc was calculated from the refractive index signal using a known sample concentration and assuming 100% mass recovery.

Thermogravimetric Analysis (TGA): TGA analyses were performed on a TA Instruments Q500 at a heating rate of 10 °C min^{-1} under nitrogen atmosphere.

Differential Scanning Calorimetry (DSC): Thermal properties of the polymers were characterized using the Mettler Toledo DSC 1 instrument under nitrogen atmosphere.

Real Time – Fourier Transform Infrared (RT-FTIR): The thiol-ene post polymerization modification kinetics of **poly(3)** were studied via RT-FTIR using a Thermo Fisher Scientific Nicolet 6700 FTIR spectrometer. A drop of the freshly prepared mixture containing **poly(3)**, thiol and Omnirad 2100 was sandwiched between two polished NaCl plates. Once the sample was exposed to UV light, spectra were recorded every 20 ms at an average of 1 scan with a spectral resolution of 16 cm^{-1}. To calculate **poly(3)** ene conversion due to UV irradiation (OmniCure S1500 Curing System, 100 mW/cm^2), the intensity reduction of C=C double bond peak at 925 cm^{-1} as compared to the initial peak was calculated. The double bond peak area was normalized to the non-reactive CH_2 stretches at 2976 cm^{-1} for the thioglycerol mixture, and 2926 cm^{-1} for the lauryl mercaptan mixture respectively.

Optical Rotation: The optical rotation was measured at 20°C in $CHCl_3$ via the Rudolph Research Analytical Autopol III Automatic Polarimeter. The measurement was performed in triplicate.

2. Preparation and Characterization of 3

Two synthetic routes were investigated for **3** as described below.

2.1 Synthetic Route 1

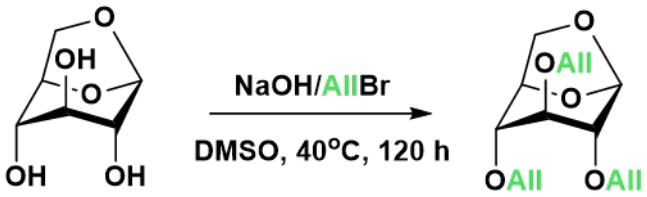

1 **3**

In a 250 mL round-bottom flask, levoglucosan (5 g, 30.84 mmol, 1 equiv.) was dissolved in dimethyl sulfoxide (30.84 mL) by stirring at room temperature. Sodium hydroxide pellets (4.07 g, 101.8 mmol, 3.3 equiv.) were ground into a fine powder. Freshly powdered sodium hydroxide was added to the levoglucosan solution while stirring at the rate of 400 rpm. The solution was heated to 40°C and allyl bromide (8.81 mL, 101.8 mmol, 3.3 equiv.) was added dropwise over the course of 15 min. One additional aliquot of powdered sodium hydroxide (3.3 equiv.) and allyl bromide (3.3 equiv.) was added to the solution at the 24 h and 48 h time points.

After 120-hour reaction, the aqueous layer was extracted with diethyl ether (3 x 200 mL). The organic layer was dried over Na_2SO_4 and the filtrate was then concentrated via rotary evaporation. The crude mixture was subjected to column chromatography on silica gel (4:1 Hexanes:EtOAc) to isolate **3** as a yellow oil (Yield = 75%).

2.2 Synthetic Route 2

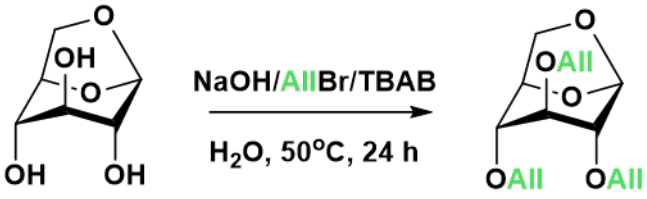

1 **3**

In a 50 mL round-bottom flask, levoglucosan (2 g, 12.34 mmol, 1 equiv.) and the phase transfer catalyst tetrabutylammonium bromide (TBAB, 240 mg, 0.74 mmol, 0.06 equiv.) were

weighed out. Sodium hydroxide pellets (2.97 g, 74.04 mmol, 6 equiv.) were dissolved in DI water (11.88 ml) to obtain a 25% NaOH aqueous solution. The levoglucosan-TBAB mixtures was dissolved in the 25% NaOH aqueous solution by stirring at room temperature. The solution was heated to 50℃ and allyl bromide (6.5 ml, 74.04 mmol, 6 equiv.) was added dropwise over the course of 15 min.

After 24-hour reaction, the aqueous layer was extracted with dichloromethane (3 x 100 mL). The organic layer was dried over Na_2SO_4 and the filtrate was then concentrated via rotary evaporation. The crude mixture was subjected to column chromatography on silica gel (4:1 Hexanes:EtOAc) to isolate **3** as a yellow oil (Yield = 36%).

^{1}H NMR (400 MHz, $CDCl_3$): δ 5.98 – 5.84 (m, 3H, -O-CH_2-C**H**=CH_2), 5.43 (s, 1H, -O-C**H**-O), 5.34 – 5.16 (m, 6H, -O-CH_2-CH=C**H_2**), 4.57 (d, J = 8 Hz, 1H), 4.17 – 4.07 (m, 6H, -O-C**H_2**-CH=CH_2), 3.92 (d, J = 4 Hz, 1H), 3.70 (t, J = 6 Hz, 1H), 3.51 (s, 1H), 3.30 (s, 1H), 3.27 (s, 1H).

^{13}C NMR (400 MHz, $CDCl_3$): δ 134.81, 134.7, 134.67, 117.76, 117.62, 117.33, 100.81, 77.36, 74.88, 71.42, 71.21, 70.64, 65.69.

HRMS (ESI-TOF): [**3** + Na]+ : calculated 305.1359; found 305.1361

3. cROP Procedure

3.1. Representative polymerization procedure of 2 in 100% CH_2Cl_2 or MeCN

In a nitrogen-filled glovebox, the required amount of catalyst (*e.g.* 0.01 mmol for 2 mol% catalyst loading) was weighed out in an 8 ml scintillation vial. A Teflon coated stir bar was added to this vial. **2** (0.5 mmol) was dissolved in CH_2Cl_2 or MeCN (*e.g.* 500 μL for initial monomer concentration of 1M) and added to the vial containing the catalyst. The vial was sealed with a Teflon lined cap and the polymerization solution was stirred at RT inside the glovebox. After 72 hours, the vial was removed from the glovebox. The polymerization was quenched with methanol (100 μL) or tert-butyl alcohol (100 μL) and stirred for an additional 10 mins. The crude reaction mixture was analyzed by ^{1}H NMR spectroscopy to determine conversion. The polymer was then precipitated twice into cold methanol. The methanol was removed, and the polymer was dried under vacuum overnight. Typical **poly(2)** yield ranged from 65 to 90%.

3.2 Representative polymerization procedure of 2 in a mixed solvent system

In a nitrogen-filled glovebox, the required amount of $Sc(OTf)_3$ (*e.g.* 0.01 mmol for 2 mol% catalyst loading) was weighed out in an 8 ml scintillation vial. MeCN (*e.g.* 50 μL for 10% MeCN) was added to the vial containing $Sc(OTf)_3$, along with a Teflon coated stir bar. **2** (0.5 mmol) was dissolved in CH_2Cl_2 (*e.g.* 450 μL for 90% CH_2Cl_2 and for total initial monomer concentration of 1M) and added to the vial containing $Sc(OTf)_3$. The vial was sealed with a Teflon lined cap and the polymerization solution was stirred at RT inside the glovebox. After 72 hours, the vial was removed from the glovebox. The polymerization was quenched with methanol (100 μL) or tert-butyl alcohol (100 μL) and stirred for an additional 10 mins. The crude reaction mixture was analyzed by ^{1}H NMR spectroscopy to determine conversion. The polymer was then precipitated

twice into cold methanol. The methanol was removed, and the polymer was dried under vacuum overnight. Typical **poly(2)** yield ranged from 37 to 68%.

3.3 ^{1}H NMR analysis for determining monomer conversion in cROP of 2

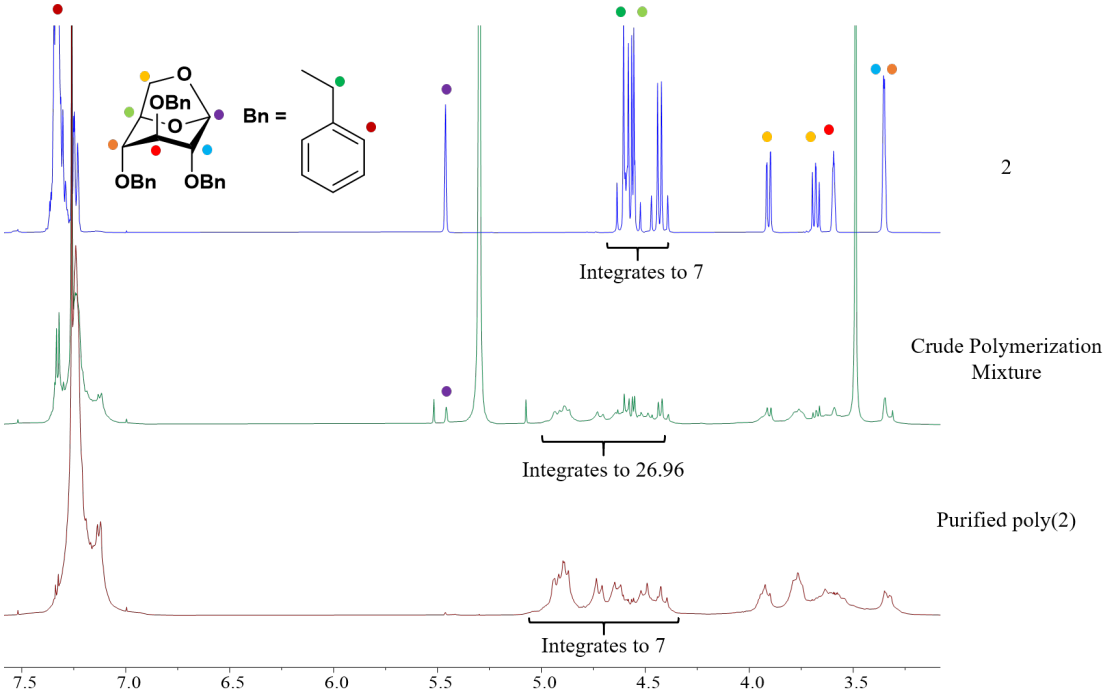

Figure S1. ^{1}H NMR spectra (400 MHz, $CDCl_3$) of monomer **2**, crude polymerization mixture of Table 1, Entry 1, and purified polymer **poly(2)**.

Monomer conversion was determined by ^{1}H NMR analysis of the crude polymerization mixture. For this purpose, the C_1 anomeric proton was used which is labeled using a purple circle in the monomer **2** and crude polymerization mixture spectra. The conversion was calculated as follows. H_P corresponds to the integration of polymer repeat unit proton and H_M corresponds to the integration of the anomeric proton in ***2***.

$$\int H_P = \frac{26.96 - 7}{7} = 2.85$$

$$Conversion = \frac{\int H_P}{\int H_P + \int H_M} = \frac{2.85}{2.85 + 1} = 0.74$$

3.4 Representative polymerization procedure of 3 in 100% CH_2Cl_2

In a nitrogen-filled glovebox, the required amount of catalyst (*e.g.* 0.017 mmol for 5 mol% catalyst loading) was weighed out in an 8 ml scintillation vial. A Teflon coated stir bar was added to this vial. **3** (0.354 mmol) was dissolved in CH_2Cl_2 (354 μL for initial monomer concentration of 1M) and added to the vial containing the catalyst. The vial was sealed with a Teflon lined cap and the polymerization solution was stirred at RT inside the glovebox. After 72 hours, the vial was removed from the glovebox. The polymerization was quenched with tert-butyl alcohol (100 μL) and stirred for an additional 10 mins. The crude reaction mixture was analyzed by ^{1}H NMR spectroscopy to determine conversion. The polymer was precipitated into a cold mixture of 50:50 water : methanol. The precipitation solvent was then removed, and the isolated polymer was redissolved in CH_2Cl_2. Water was removed by drying over Na_2SO_4, followed by rotary evaporation of the filtrate and finally drying the polymer under vacuum overnight. Typical **poly(3)** yield ranged from 38 to 91%.

3.5 Representative polymerization procedure of 3 in a mixed solvent system

In a nitrogen-filled glovebox, the required amount of $Bi(OTf)_3$ (*e.g.* 0.017 mmol for 5 mol% catalyst loading) was weighed out in an 8 ml scintillation vial. MeCN (*e.g.* 35.4 μL for 10% MeCN) was added to the vial containing $Sc(OTf)_3$, along with a Teflon coated stir bar. **3** (0.354 mmol) was dissolved in CH_2Cl_2 (318.6 μL for 90% CH_2Cl_2 and for initial monomer concentration of 1M) and added to the vial containing $Bi(OTf)_3$. The vial was sealed with a Teflon lined cap and the polymerization solution was stirred at RT inside the glovebox. After 72 hours, the vial was removed from the glovebox. The polymerization was quenched with tert-butyl alcohol (100 μL) and stirred for an additional 10 mins. The crude reaction mixture was analyzed by ^{1}H NMR spectroscopy to determine conversion. The polymer was precipitated into a cold mixture of 50:50

water : methanol. The precipitation solvent was then removed, and the isolated polymer was redissolved in CH_2Cl_2. Water was removed by drying over Na_2SO_4, followed by rotary evaporation of the filtrate and finally drying the polymer under vacuum overnight. Typical **poly(3)** yield ranged from 53 to 87%.

3.6 ^{1}H NMR analysis for determining monomer conversion in cROP of 3

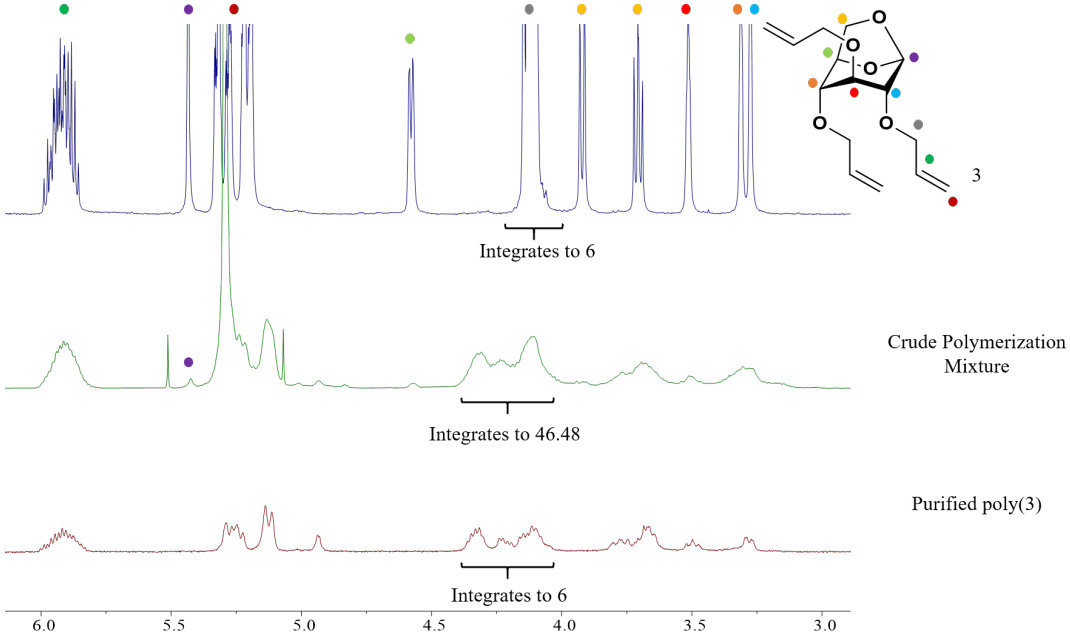

Figure S2. ^{1}H NMR spectra (400 MHz, $CDCl_3$) of monomer **3**, crude polymerization mixture of Table 1, Entry 6, and purified polymer **poly(3).**

Monomer conversion was determined by ^{1}H NMR analysis of the crude polymerization mixture. For this purpose, the C_1 anomeric proton was used which is labeled using a purple circle in the monomer ***3*** and crude polymerization mixture spectra. The conversion was calculated as follows. H_P corresponds to the integration of polymer repeat unit proton and H_M corresponds to the integration of the anomeric proton in **3**.

$$\int H_P = \frac{46.48 - 6}{6} = 6.75$$

$$Conversion = \frac{\int H_P}{\int H_P + \int H_M} = \frac{6.75}{6.75 + 1} = 0.86$$

4. cROP Screening Results

4.1 Catalyst Screening

4.1.1 Structures of catalysts

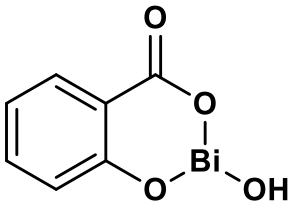

Bismuth subsalicylate

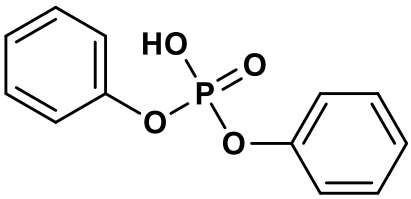

Diphenyl phosphoric acid

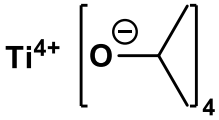

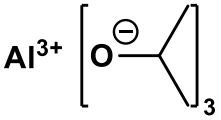

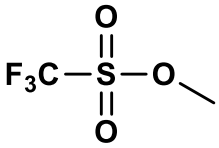

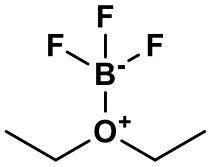

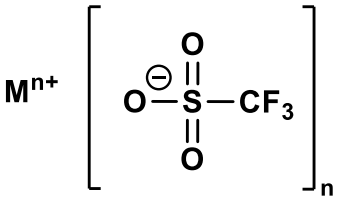

M = Al, Zn, Fe, Bi, Sc, La, Y

Figure S3. Structure of cROP catalysts used in this study.

4.1.2 Results

Table S1. Summary of cROP catalyst screening for 2 and 3, green indicates non-zero conversion. [a]Polymerization conditions for 2: $[2]_0$ = 1M in CH_2Cl_2 at 25℃, 2:Cat = 50:1, time = 72h. [b]Polymerization conditions for 3: $[3]_0$ = 1M in CH_2Cl_2 at 25℃, 3:Cat = 20:1, time = 72h. . Red = zero conversion; Green = non-zero conversion; NA = Not applicable.

Catalyst	2[a]	3[b]
Bismuth subsalicylate		NA

Diphenyl phosphoric acid		NA
$Ti(iOPr)_4$		NA
$Al(iOPr)_3$		NA
BF_3OEt_2		
MeOTf		
$Fe(OTf)_3$		NA
$Sc(OTf)_3$		
$Al(OTf)_3$		NA
$Bi(OTf)_3$		
$La(OTf)_3$		NA
$Y(OTf)_3$		NA
$Zn(OTf)_2$		NA

Table S2. Results of hit cROP catalysts for 2 and 3. Polymerizations were performed for 72h in CH_2Cl_2 at RT, $[2]_0$ = 1M, and $[3]_0$ = 1M. [a]Monomer conversion by ^1H NMR spectroscopy. [b]Molecular weights and dispersity determined by SEC-MALS in DMF.

Monomer	Catalyst	Monomer : Catalyst	Conversion[a] (%)	M_n[b] (g/mol)	M_w[b] (g/mol)	Đ[b]
2	BF_3OEt_2	50 : 1	66	8700	14500	1.7
2	MeOTf	50 : 1	70	4300	6300	1.5
2	$Sc(OTf)_3$	50 : 1	74	6700	11030	1.6
2	$Bi(OTf)_3$	50 : 1	84	3500	4400	1.3
3	MeOTf	20 : 1	92	3600	9100	2.5
3	$Sc(OTf)_3$	20 : 1	77	3500	7900	2.3
3	$Bi(OTf)_3$	20 : 1	86	3600	6100	1.7

4.2 Solvent Screening

Table S3. Summary of cROP solvent screening for 2 and 3, green indicates non-zero conversion. [a]Polymerization conditions for 2: $[2]_0$ = 1M at 25°C, 2:$Sc(OTf)_3$ = 50:1, time = 72h. [b]Polymerization conditions for 3: $[3]_0$ = 1M at 25°C, 3:$Bi(OTf)_3$ = 20:1, time = 72h. Red = zero conversion; Green = non-zero conversion; NA = Not applicable.

Solvent CH_2Cl_2 : MeCN	2[a]	3[b]
100 : 0		
0 : 100		NA
50 : 50		NA
80 : 20		NA
90 : 10		
99 : 1		

Table S4. Results of hit cROP solvent systems for 2 and 3. Polymerizations were performed for 72h at RT, $[2]_0$ = 1M, and $[3]_0$ = 1M. [a]Monomer conversion by ^{1}H NMR spectroscopy. [b]Molecular weights and dispersity determined by SEC-MALS in DMF.

Monomer	Catalyst	Solvent CH_2Cl_2 : MeCN	Monomer : Catalyst	Conversion[a] (%)	M_n[b] (g/mol)	M_w[b] (g/mol)	Đ[b]
2	$Sc(OTf)_3$	100 : 0	50 : 1	74	6700	11030	1.6
2	$Sc(OTf)_3$	99 : 1	50 : 1	66	8800	12500	1.43
2	$Sc(OTf)_3$	90 : 10	50 : 1	58	9630	12700	1.32
3	$Bi(OTf)_3$	100 : 0	20 : 1	86	3600	6100	1.7
3	$Bi(OTf)_3$	99 : 1	20 : 1	89	3400	5020	1.6
3	$Bi(OTf)_3$	90 : 10	20 : 1	74	2300	3000	1.3

4.3 Catalyst loading and initial monomer concentration

Table S5. Additional results of varying catalyst loading and initial monomer concentration on cROP of 2. [a]Monomer conversion by ^{1}H NMR spectroscopy. [b]Molecular weights and dispersity determined by SEC-MALS in DMF. Polymerization conditions : $Sc(OTf)_3$ catalyst, 72h, RT.

Solvent CH_2Cl_2 : MeCN	Monomer Concentration (M)	Monomer : Catalyst	Conversion[a] (%)	M_n[b] (g/mol)	M_w[b] (g/mol)	Đ[b]
100 : 0	1	100 : 1	68	4100	8530	2.1
100 : 0	1	333 : 1	0	-	-	-
99 : 1	1	100 : 1	28	7100	9060	1.3
99 : 1	2	1000 : 1	0	-	-	-

5. Polymerization Kinetics

5.1 Overall cROP kinetics of monomer 2

In a nitrogen-filled glovebox, 4.27 mg of $Sc(OTf)_3$ (0.009 mmol for 0.5 mol% catalyst loading) was weighed out in an 8 ml scintillation vial. A Teflon coated stir bar was added to this vial. 750 mg of **2** (1.74 mmol) was dissolved in CH_2Cl_2 (870 μL for initial monomer concentration of 2M) and added to the vial containing the catalyst. The vial was sealed with a Teflon lined cap and the polymerization solution was stirred at RT inside the glovebox. At each specified time point, an aliquot was taken from this reaction mixture inside the glovebox and was quenched by adding methanol. The crude reaction mixture was analyzed by ^1H NMR spectroscopy to determine conversion. This study was done in triplicate.

Table S6. Conversion vs time data for each replicate

Time point (h)	Conversion (%) Replicate 1	Conversion (%) Replicate 2	Conversion (%) Replicate 3
1	19	24	32
2.5	35	45	37
4	42	50	43
8	50	57	53
10	53	53	53
24	64	68	56
28	64	63	61
31	65	67	66
48	65	66	60
74	68	70	69
124	67	70	68
144	70	76	72

5.2 Determination of rate law for cROP of 2

Based on the results of the previous study, it was decided that conversion data between 0 and 4 h will be utilized to evaluate the reaction order for cROP of **2**. To obtain sufficient time points within this region, the kinetic study was repeated in duplicate for a total reaction time of 3 h. In a nitrogen-filled glovebox, 5.13 mg of $Sc(OTf)_3$ (0.0104 mmol for 0.5 mol% catalyst loading) was weighed out in an 8 ml scintillation vial. A Teflon coated stir bar was added to this vial. 900 mg of **2** (2.08 mmol) was dissolved in CH_2Cl_2 (1040 μL for initial monomer concentration of 2M) and added to the vial containing the catalyst. The vial was sealed with a Teflon lined cap and the polymerization solution was stirred at RT inside the glovebox. At each specified time point, an aliquot was taken from this reaction mixture inside the glovebox and was quenched by adding isopropanol. The crude reaction mixture was analyzed by ^1H NMR spectroscopy to determine conversion.

Table S7. Conversion vs time data for each replicate

Time point (min)	Conversion (%) Replicate 1	Conversion (%) Replicate 2
0	0	0
5	0	0
20	5	8
30	12	17
45	17	28
65	29	33
75	33	38
90	33	40
105	37	42
120	38	43
135	38	46
150	44	47

165	47	51
180	44	44

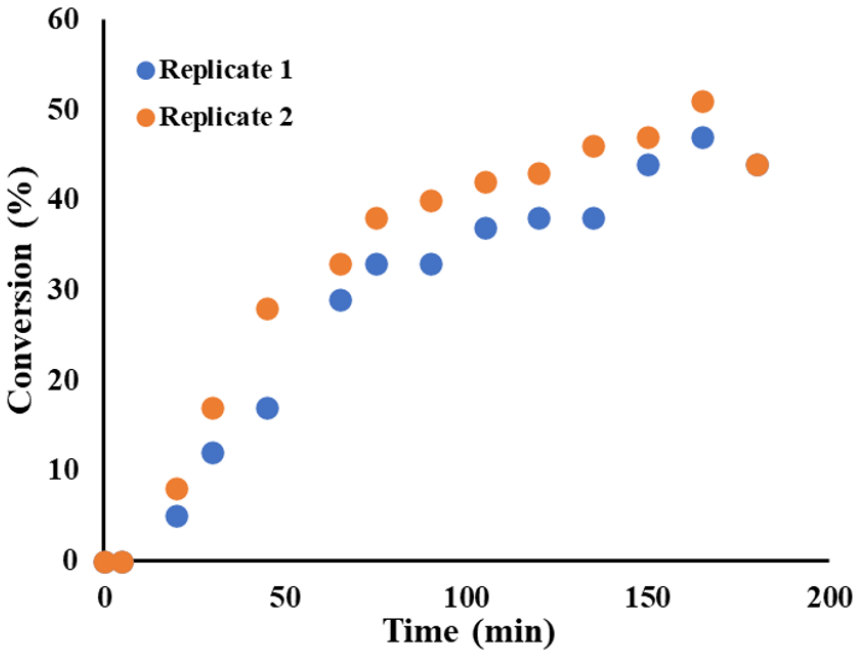

Figure S4. Conversion vs time plot for each replicate

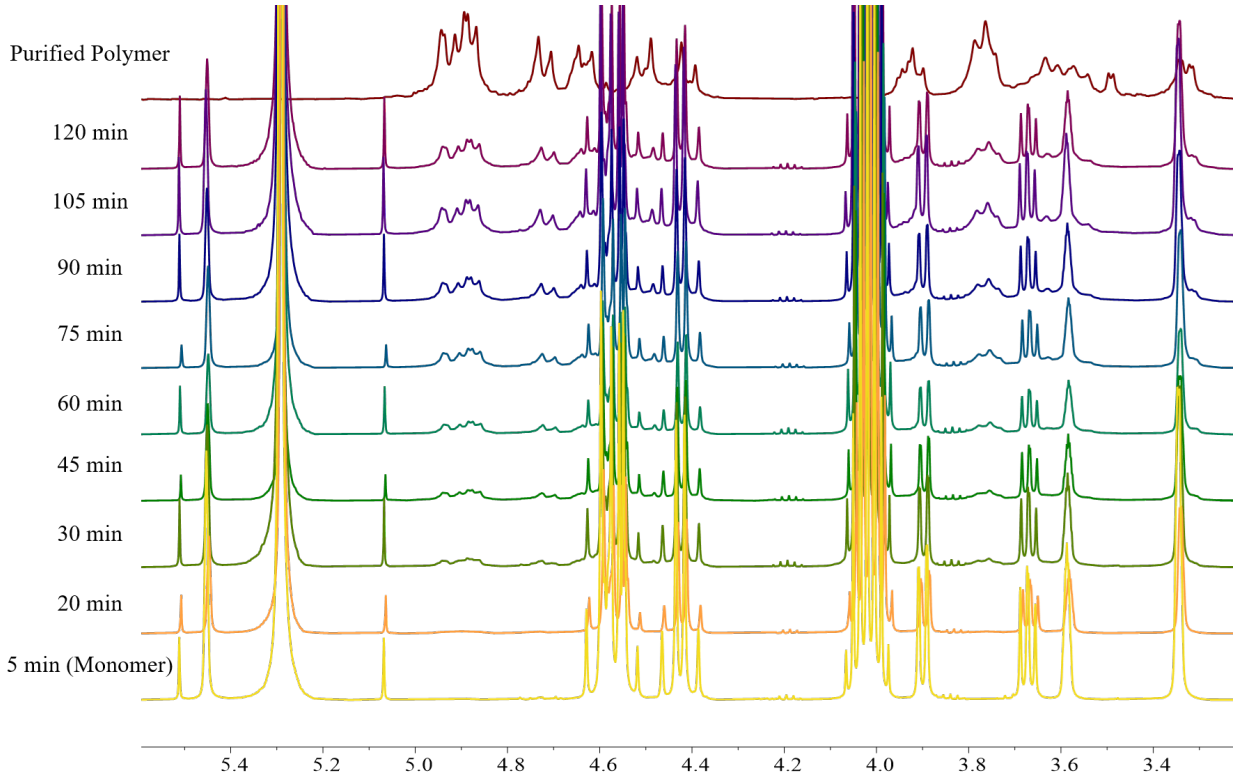

Figure S5. Kinetic study of cROP of **2** by ^{1}H NMR (400 MHz, $CDCl_3$)

5.3 Fitting plots to determine rate law for cROP kinetics of 2

To investigate whether the cROP of 2 follows zero, first or second order kinetics with respect to monomer concentration, the following plots were constructed.

Zero Order Kinetics

For zero order kinetics, a plot of $[M]_t$ vs t should be linear. $[M]_t$ was determined from conversion using the following equations:

$$\text{Conversion} = \frac{[M]_0 - [M]_t}{M_0}$$

$$[M]_t = [M]_0 * (1 - \text{conversion})$$

First Order Kinetics

For first order kinetics, a plot of $ln\frac{[M]_0}{[M]_t}$ vs t should be linear.

$$ln\frac{[M]_0}{[M]_t} = -ln\,(1 - conversion)$$

Second Order Kinetics

For second order kinetics, a plot of $\frac{1}{[M]_t}$ vs t should be linear.

$$\frac{1}{[M]_t} = \frac{1}{[M]_0 * (1 - \text{conversion})}$$

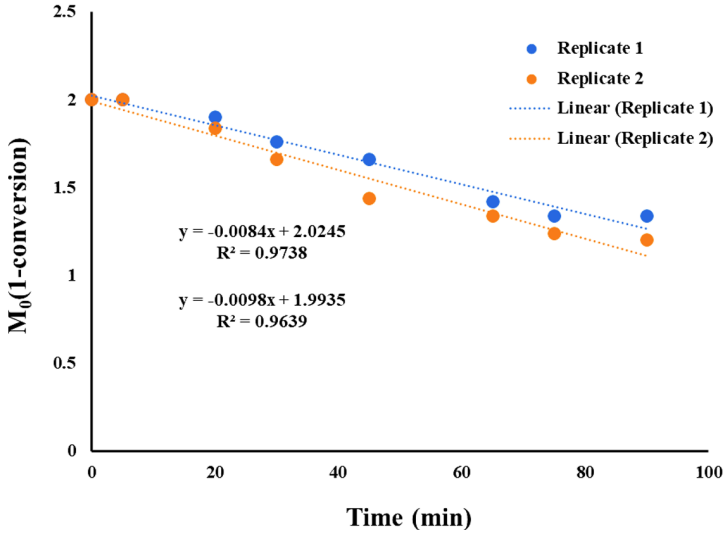

Figure S6. Zero order fit for cROP of **2**

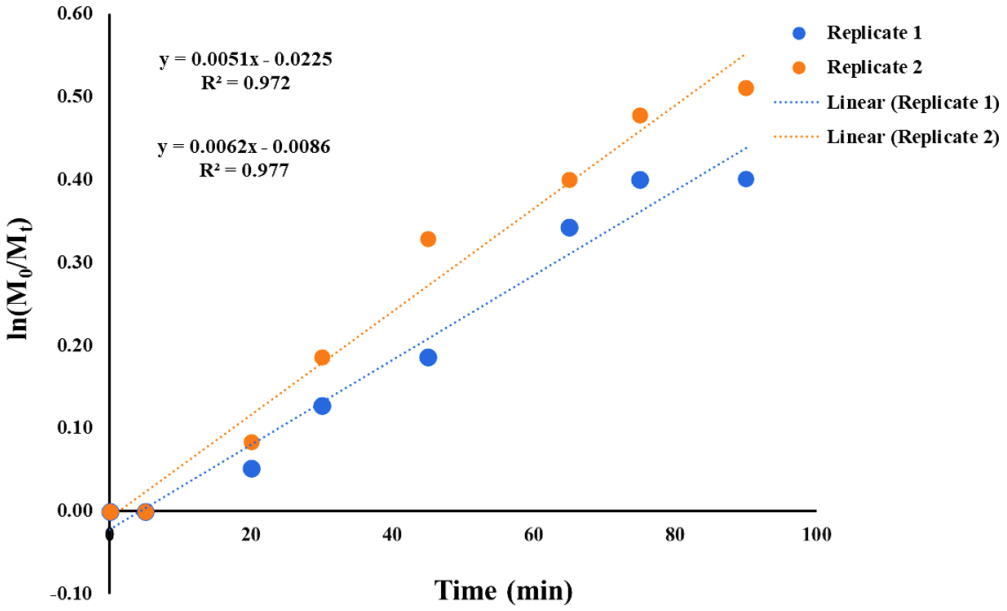

Figure S7. First order fit for cROP of **2**

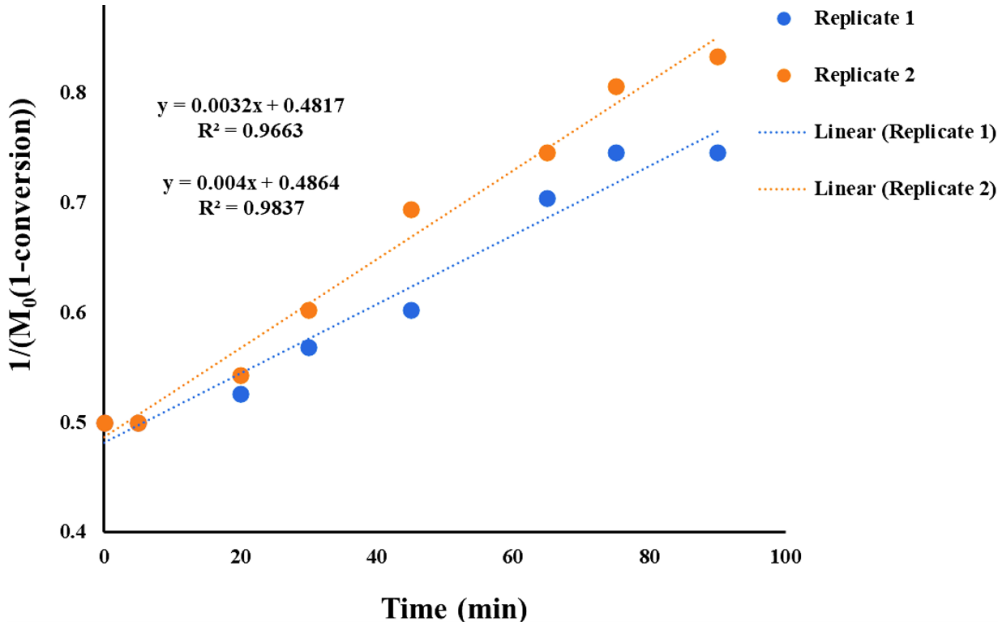

Figure S8. Second order fit for cROP of **2**

For cROP of **2**, k_{obs} could not be calculated and it is hypothesized that the cROP kinetics for **2** may follow more complex rate laws.

5.4 Overall cROP kinetics of monomer 3

In a nitrogen-filled glovebox, 28 mg of $Bi(OTf)_3$ (0.043 mmol for 1 mol% catalyst loading) was weighed out in an 8 ml scintillation vial. A Teflon coated stir bar was added to this vial. 1.2 g of **3** (4.27 mmol) was dissolved in CH_2Cl_2 (610 µL for initial monomer concentration of 7M) and added to the vial containing the catalyst. The vial was sealed with a Teflon lined cap and the polymerization solution was stirred at RT inside the glovebox. At each specified time point, an aliquot was taken from this reaction mixture inside the glovebox and was quenched by adding isopropanol. The crude reaction mixture was analyzed by ^1H NMR spectroscopy to determine conversion. This study was done in triplicate.

Table S8. Conversion vs time data for each replicate

Time point (min or h)	Conversion (%) Replicate 1	Conversion (%) Replicate 2	Conversion (%) Replicate 3
0 min	0	0	0
15 min	0	0	0
30 min	0	0	0
45 min	0	0	0
60 min	0	0	0
75 min	0	0	0
90 min	0	0	0
105 min	0	0	0
120 min	0	0	0
180 min	0	0	0
4 h	6.3	6.3	5
6 h	11	11	9
22 h	55	55	57
24 h	57	55	55
32 h	63	65	67

49 h	75	74	78
73 h	83	85	83
121 h	79	93	83
144.5 h	90	94	91

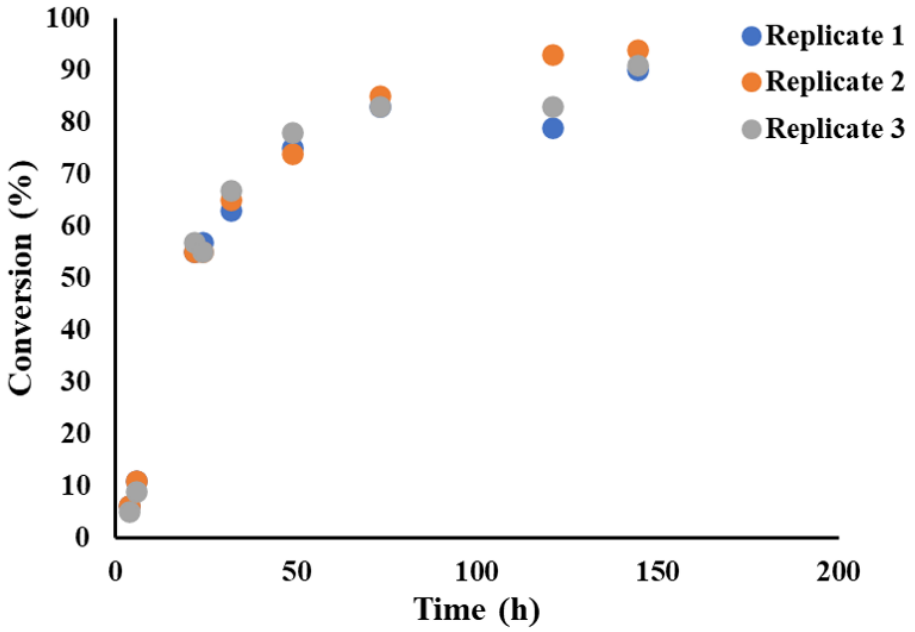

Figure S9. Conversion vs time plot for each replicate

Figure S10. Photograph depicting color change in the polymerization solution for all the replicates as a function of time. The left most vial corresponds to the 0 min time point, and the right most vial corresponds to the 4 h time point.

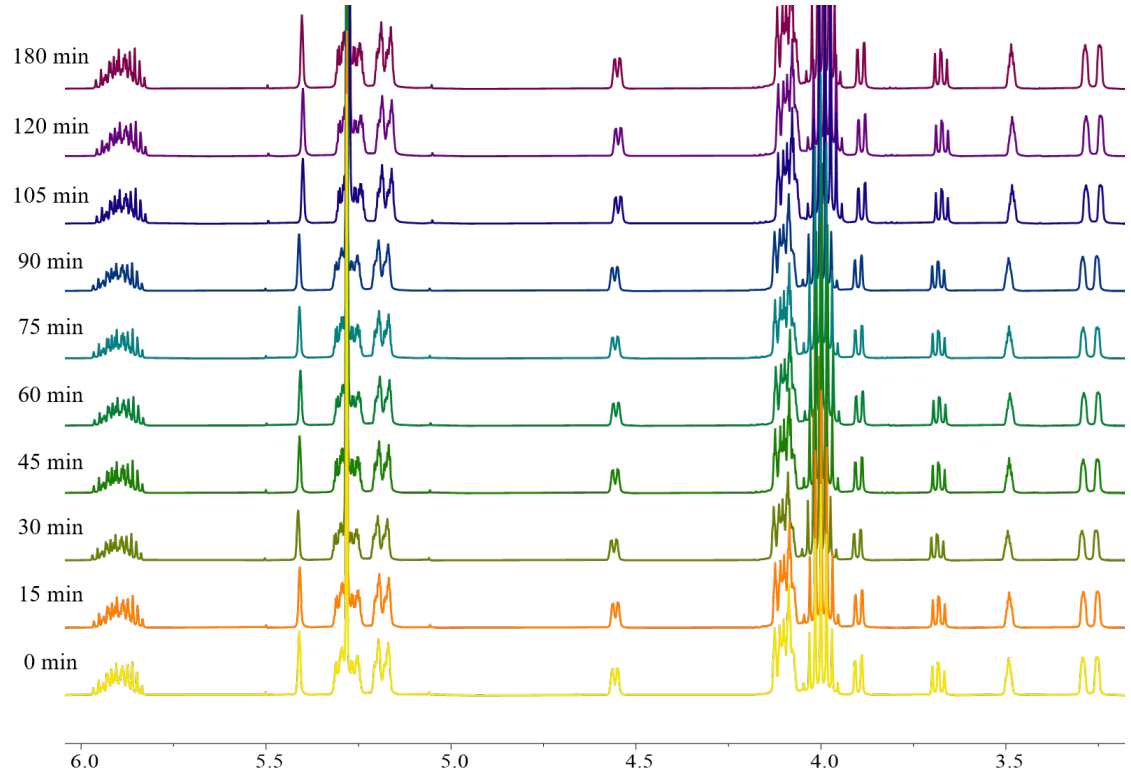

Figure S11. ^{1}H NMR (400 MHz, $CDCl_3$) spectrums for time points 0 min to 3 h depicting no polymerization within the first 3 h despite of the color change in polymerization solution.

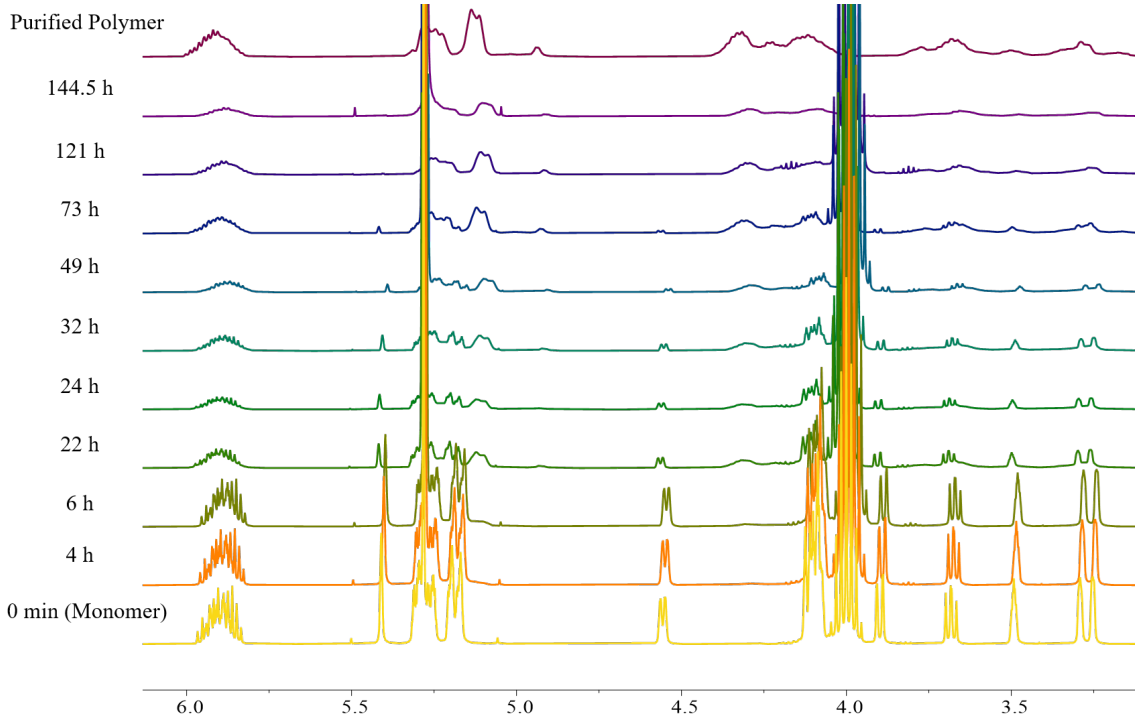

Figure S12. Kinetic study of cROP of **3** by ^{1}H NMR (400 MHz, $CDCl_3$)

5.5 Fitting plots to determine rate law for cROP kinetics of 3

To investigate whether the cROP of 3 follows zero, first or second order kinetics with respect to monomer concentration, the following plots were graphed as described in section 5.3.

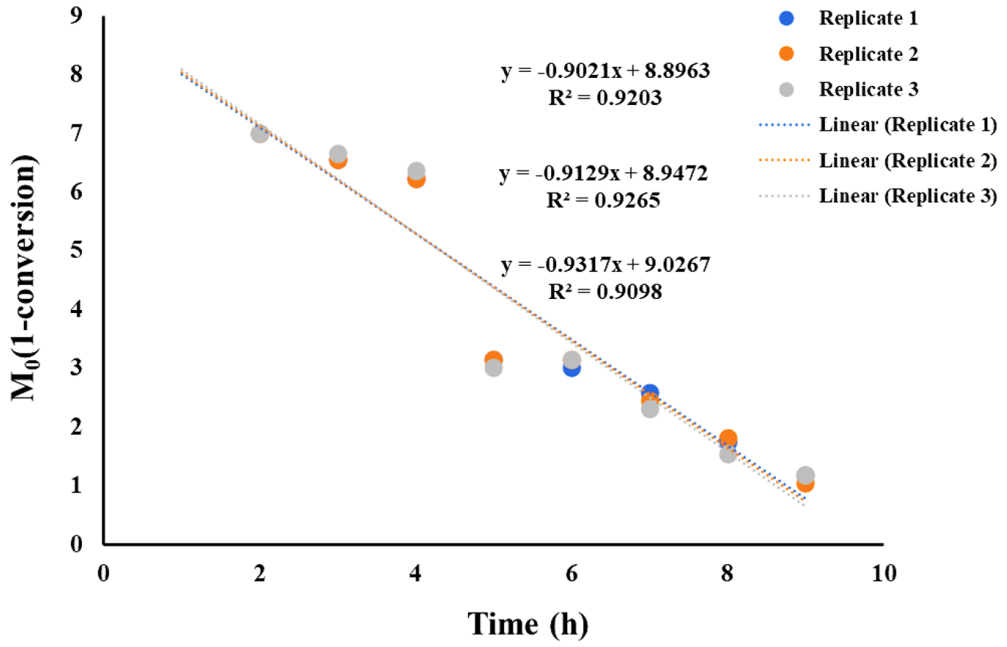

Figure S13. Zero order fit for cROP of **3**

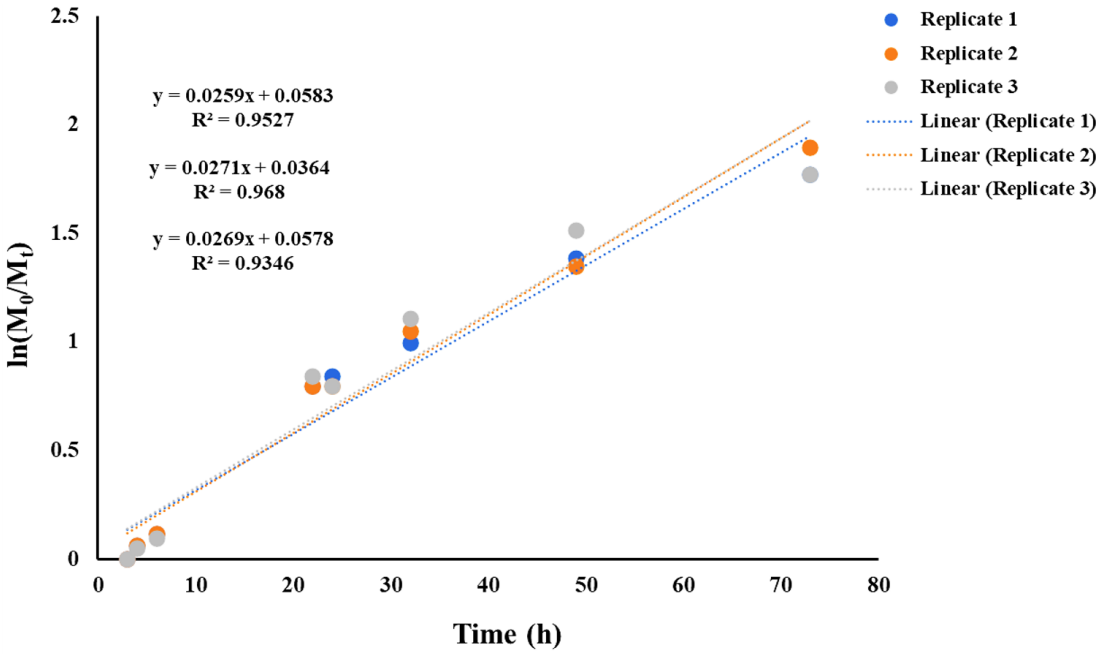

Figure S14. First order fit for cROP of **3**

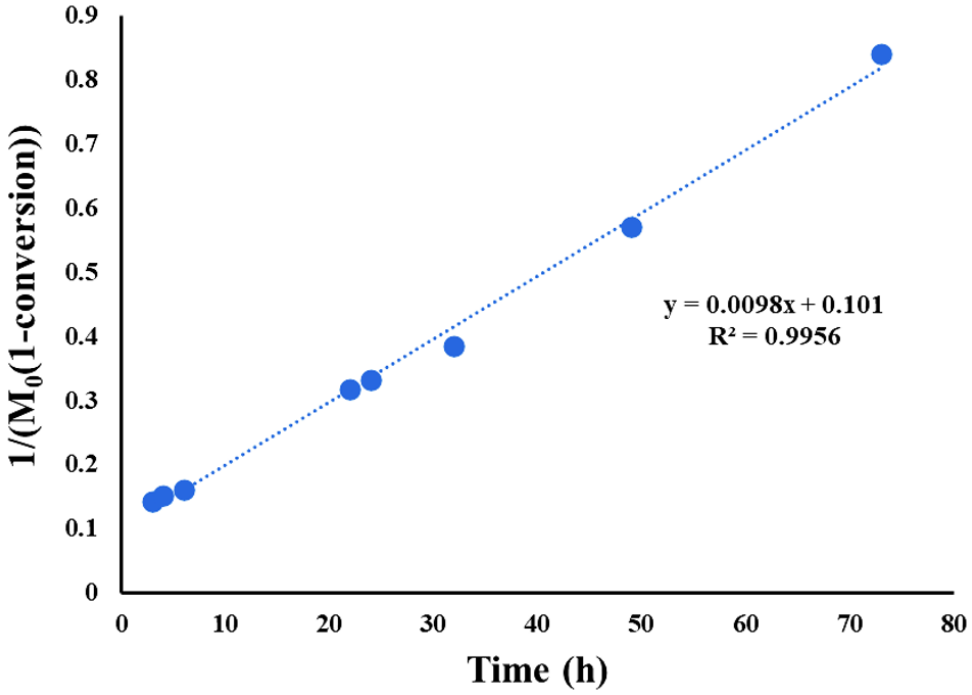

Figure S15. Second order fit for replicate 1 in cROP of **3**.

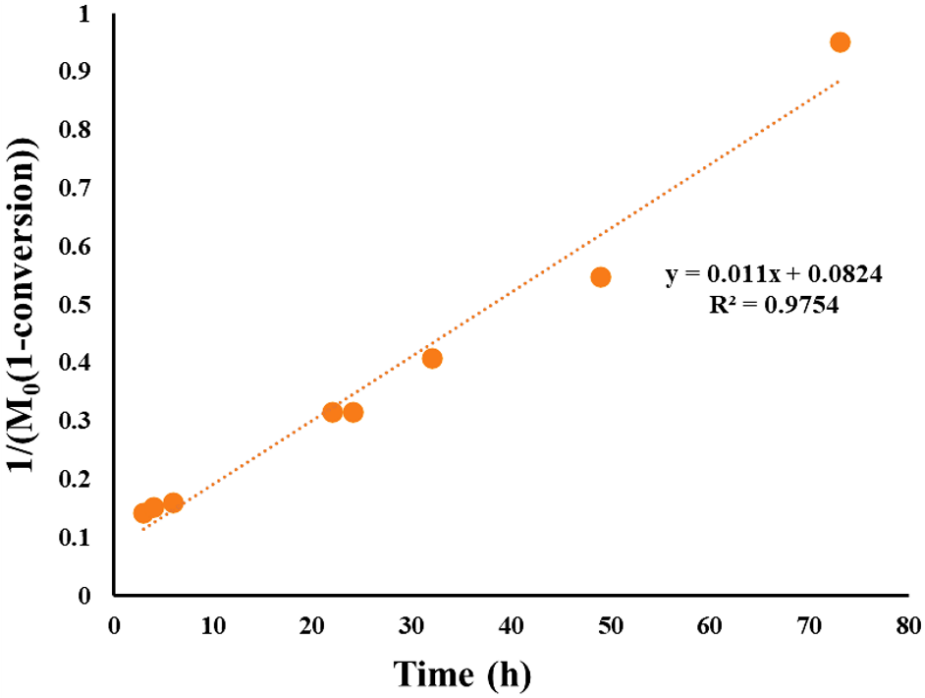

Figure S16. Second order fit for replicate 2 in cROP of **3**.

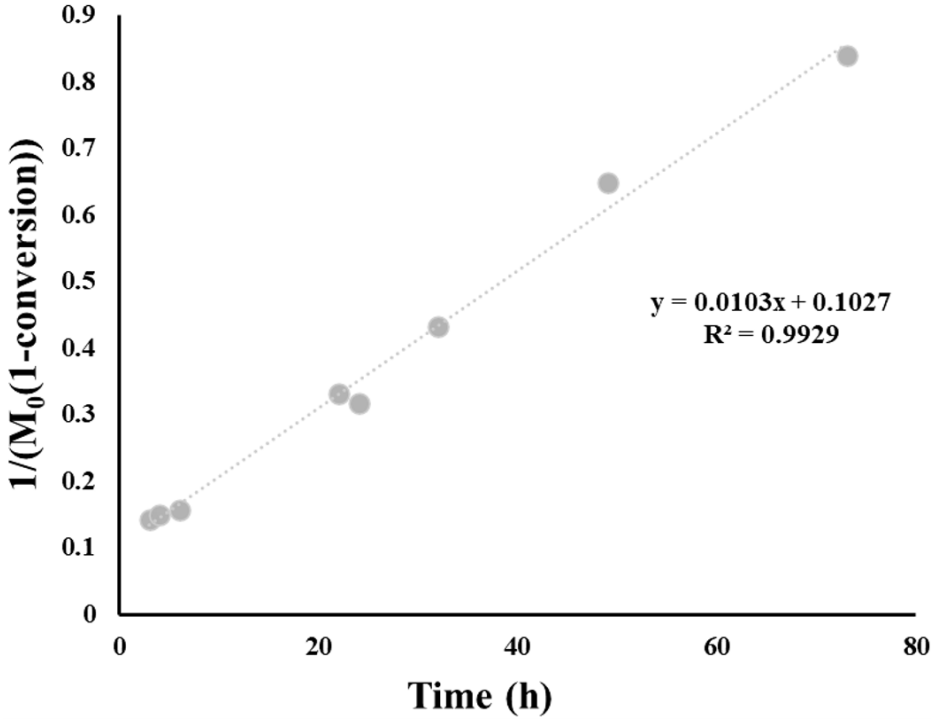

Figure S17. Second order fit for replicate 3 in cROP of **3**.

The fitting results for **3** indicated a second order rate law with respect to monomer concentration and a k_{obs} of 0.0104 $M^{-1}h^{-1}$ was determined for this monomer.

5.6 M_n vs Conversion for cROP kinetics of 2 and 3

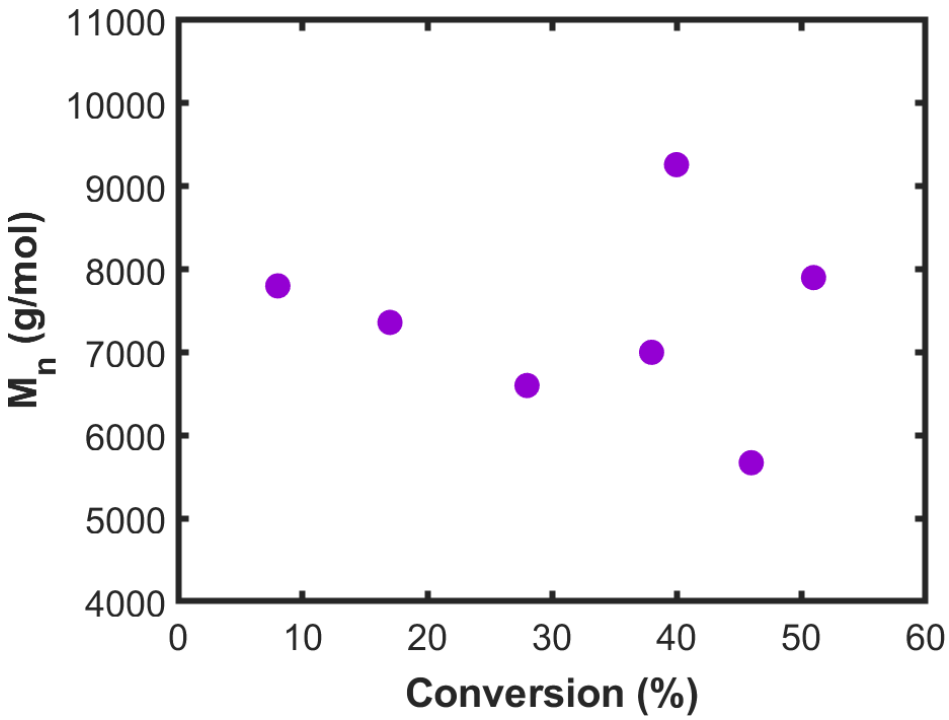

Figure S18. Plot of M_n vs Conversion for cROP of 2

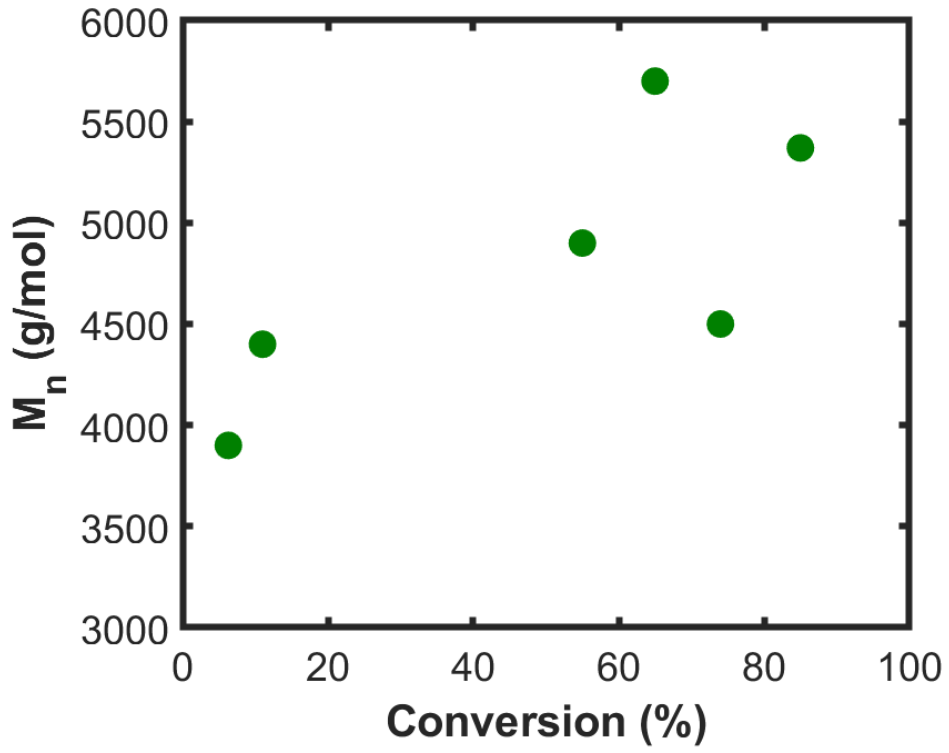

Figure S19. Plot of M_n vs Conversion for cROP of 3

5.7 *Đ* vs Conversion for cROP kinetics of 2 and 3

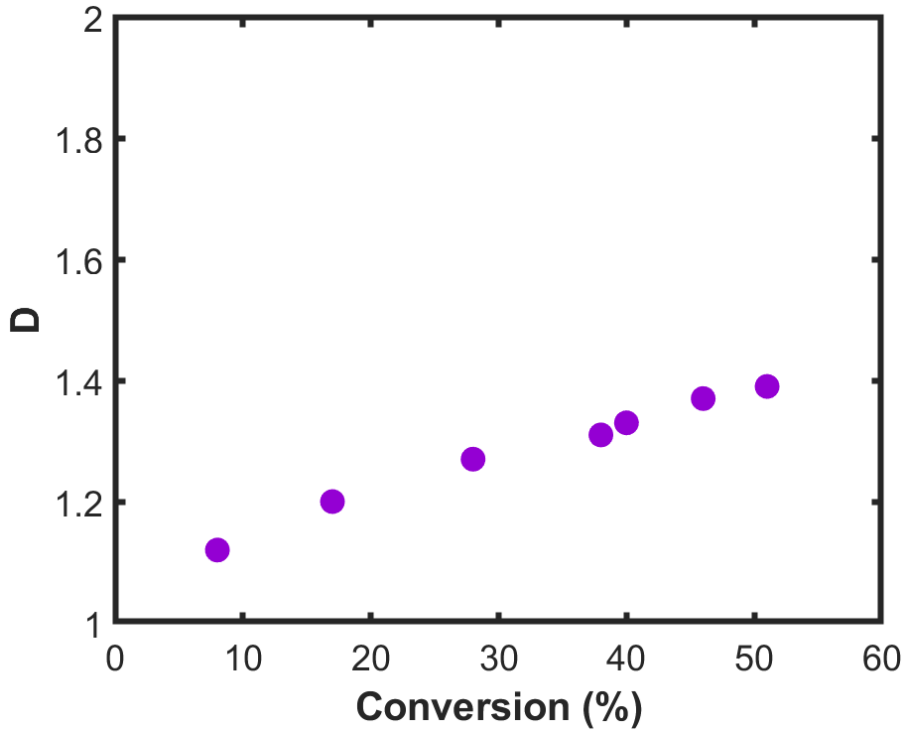

Figure S20. Plot of *Đ* vs Conversion for cROP of 2

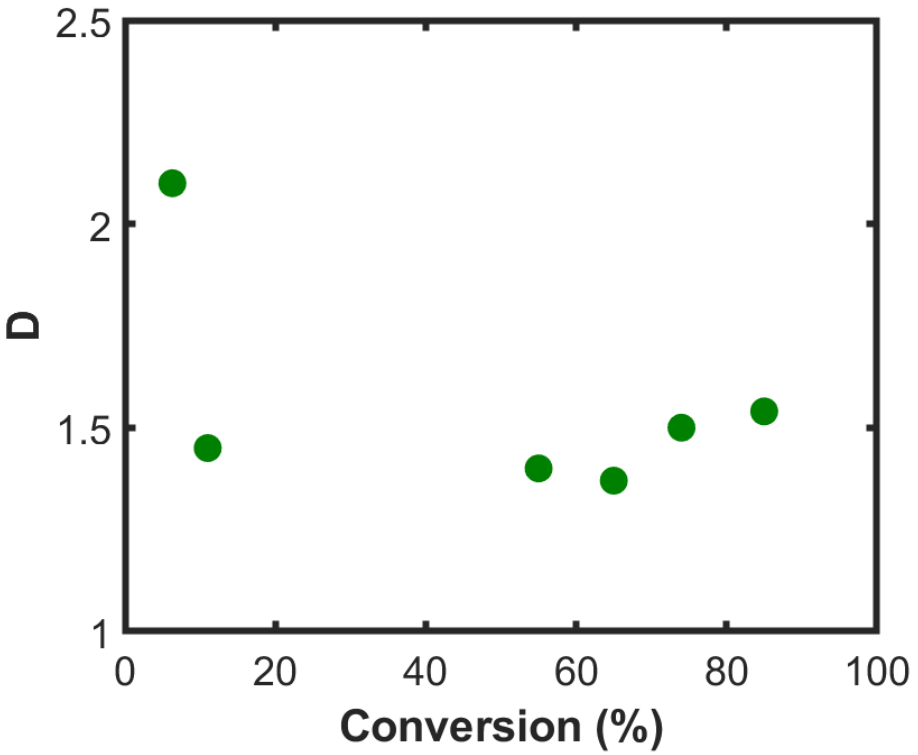

Figure S21. Plot of *Đ* vs Conversion for cROP of 3

6. Post polymerization modification of poly(3)

6.1 Synthesis and Purification of poly(4)

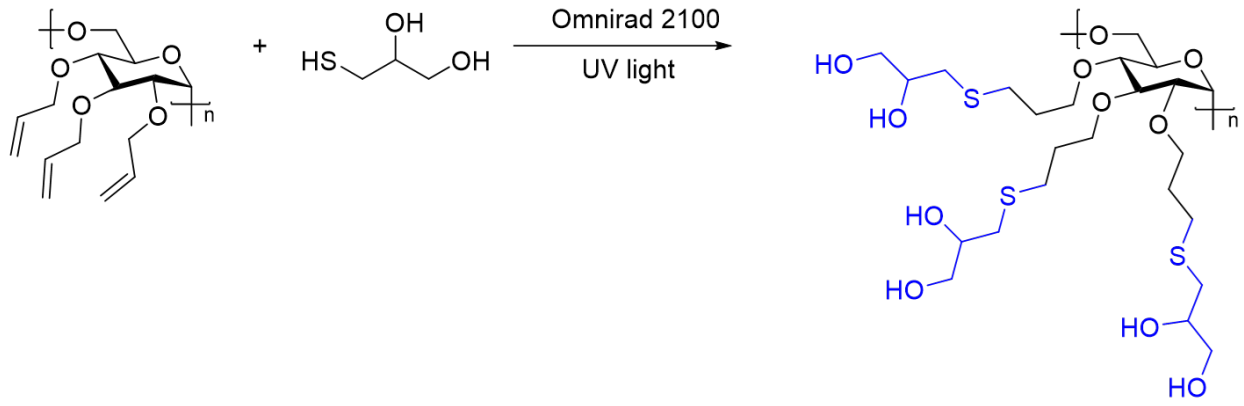

poly(3) **poly(4)**

In a 4 mL vial, **poly(3)** (100 mg, M_n = 6760 Da, f_{ene} = 72, 0.015 mmol, 1 equiv.) was dissolved in ethanol (750 µL) by vortexing at room temperature. In a separate 4 mL vial, Omnirad 2100 (19.6 mg, 9 wt% of total formulation weight) and thioglycerol (117.5 mg, f_{thiol} = 1, 1.08 mmoles, 72 equiv.) were weighed out to maintain an alkene:thiol of 1 : 1. The solution of **poly(3)** in ethanol was then added to the vial containing thioglycerol and further mixed by vortexing at room temperature. The formulation was irradiated with UV light (OmniCure S1500 Curing System, 100 mW/cm^2) for 10 min to synthesize **poly(4)**.

poly(4) was isolated from the crude mixture via a two-step purification method. In the first step, the crude mixture was redissolved in excess water and extracted thrice with dichloromethane to remove unreacted **poly(3)**. The aqueous layer was then dialyzed in water (1 kDa RC dialysis tubing) to remove any unreacted thioglycerol. The purified polymer was concentrated by rotary evaporation and finally the polymer was dried under vacuum for 48 h.

6.2 Synthesis and Purification of poly(5)

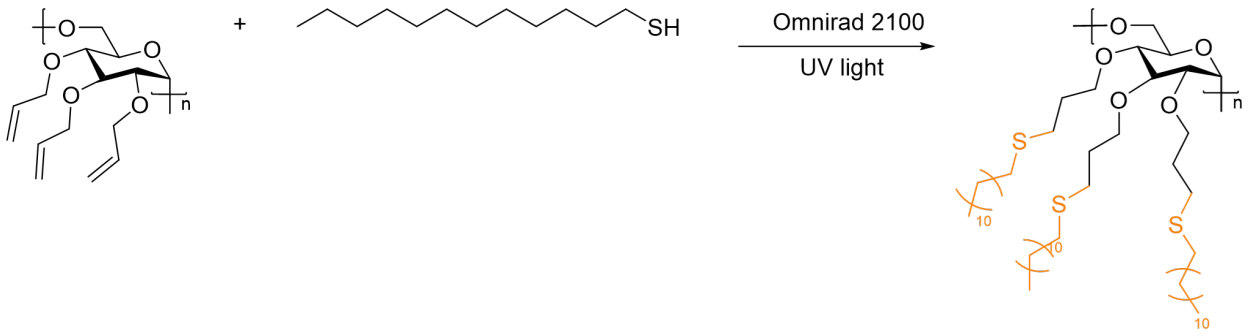

poly(3) poly(5)

In a 4 mL vial, **poly(3)** (100 mg, M_n = 6760 Da, f_{ene} = 72, 0.015 mmol, 1 equiv.) was dissolved in dichloromethane (750 µL) by vortexing at room temperature. In a separate 4 mL vial, Omnirad 2100 (28.7 mg, 9 wt% of total formulation weight) and lauryl mercaptan (218.6 mg, f_{thiol} = 1, 1.08 mmoles, 72 equiv.) were weighed out to maintain an alkene:thiol of 1 : 1. The solution of **poly(3)** in dichloromethane was then added to the vial containing lauryl mercaptan and further mixed by vortexing at room temperature. The formulation was irradiated with UV light (OmniCure S1500 Curing System, 100 mW/cm^2) for 10 min to synthesize **poly(5)**.

poly(5) was isolated from the crude mixture by dialysis in dichloromethane (6 to 8 kDa RC dialysis tubing) to remove unreacted **poly(3)**. The purified polymer was concentrated by rotary evaporation and finally the polymer was dried under vacuum overnight.

6.3 RT-FTIR spectra for poly(4)

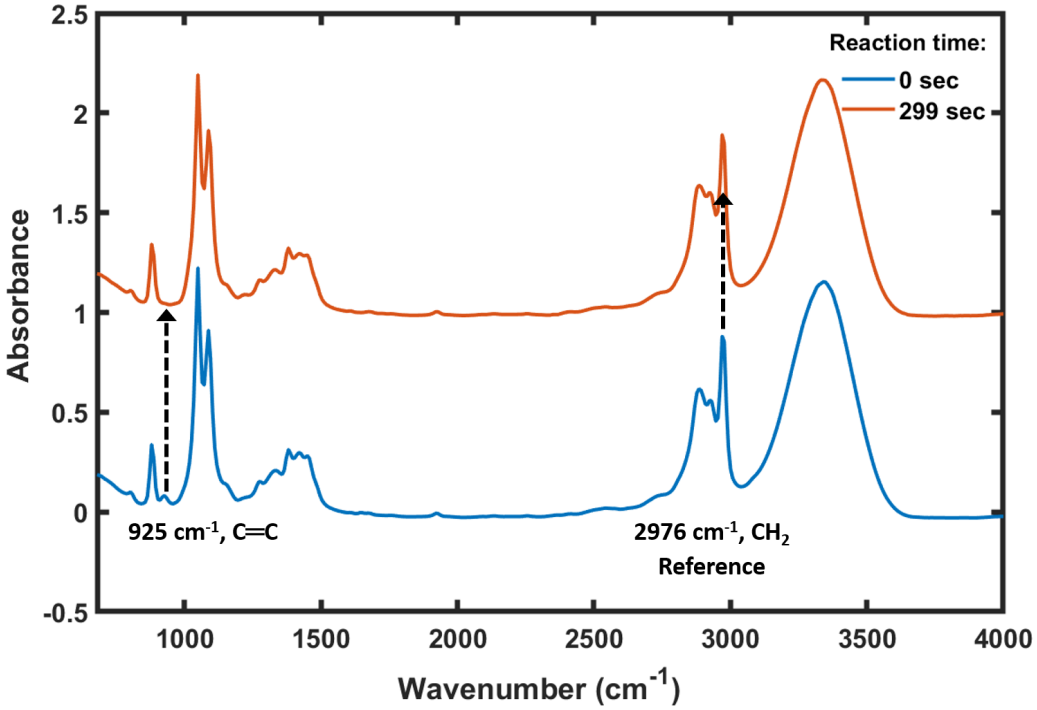

Figure S22. FTIR spectra for **poly(3)**-thioglycerol as a function of irradiation time.

6.4 RT-FTIR spectra for poly(5)

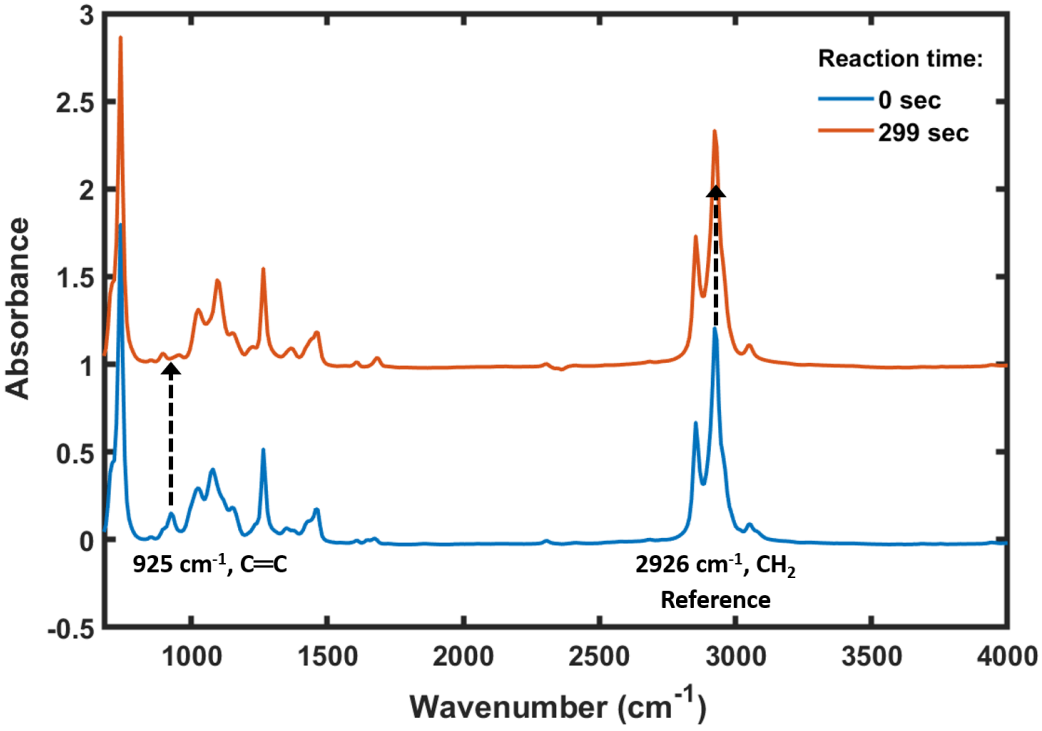

Figure S23. FTIR spectra for **poly(3)**-lauryl mercaptan as a function of irradiation time.

6.5 SEC analysis of poly(4) and poly(5)

Table S9 SEC analysis of **poly(3)** after post-polymerization modification

Polymer	poly(3)	poly(4)	poly(5)
M_n	6.76 kDa	27 kDa	25.4 kDa
M_w	10.5 kDa	31.4 kDa	37.3 kDa
$Đ$	1.54	1.2	1.47

7. Solubility of Polymers

poly(2) is soluble in solvents with intermediate polarity, whereas **poly(3)** is soluble in all tested solvents except water. As expected, **poly(4)** and **poly(5)** display starkly different solubility properties owing to the contrast in hydrophilicity. **poly(4)** is the only water-soluble polymer in the synthesized library, whereas **poly(5)** is insoluble in highly polar alcohols and DMF. Notably, most of the levoglucosan based polysaccharides are soluble in less hazardous solvents such as methyl tert-butyl ether, and green solvents such as acetone and ethyl acetate.

Table S10 Solubility test of polymers in solvents with different polarities

Polymer/ Solvent	poly(2)	poly(3)	poly(4)	poly(5)	ε at 20°C
Hexanes	✗	✓	✗	✓	1.9
MTBE	✓	✓	✗	✓	4.5
$CHCl_3$	✓	✓	✗	✓	4.8
EtOAc	✓	✓	✗	✓	6.02
THF	✓	✓	✗	✓	7.6
CH_2Cl_2	✓	✓	✗	✓	9.1
Acetone	✓	✓	✗	✓	20.6
Ethanol	✗	✓	✓	✗	22.4
Methanol	✗	✓	✓	✗	32.6
DMF	✓	✓	✓	✗	36.7
Water	✗	✗	✓	✗	79.7

8. DSC Traces

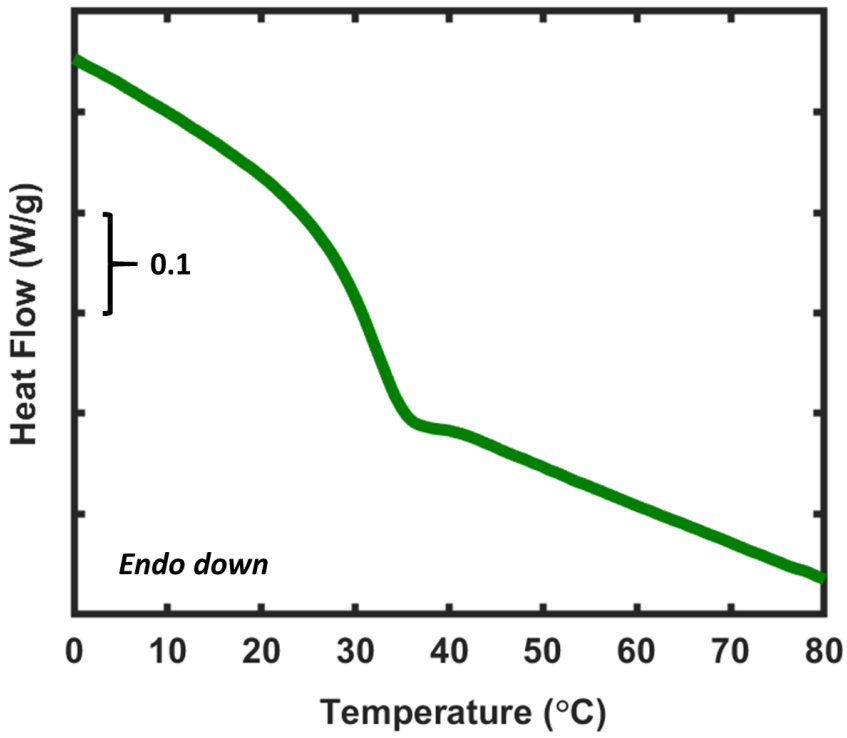

Figure S24. DSC thermogram (second heating, 10 °C/min) for **poly(2)**.

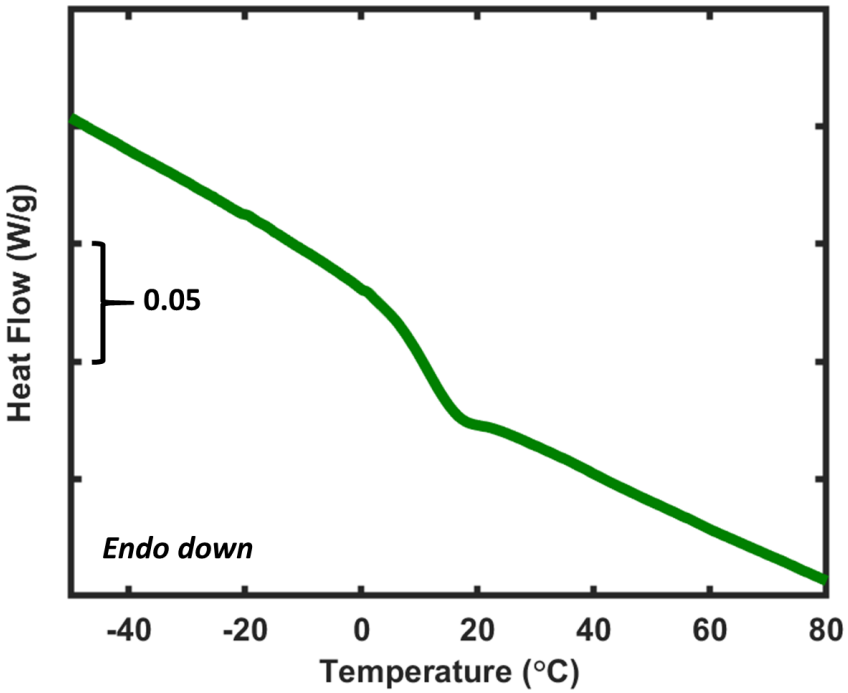

Figure S25. DSC thermogram (second heating, 10 °C/min) for **poly(3)**.

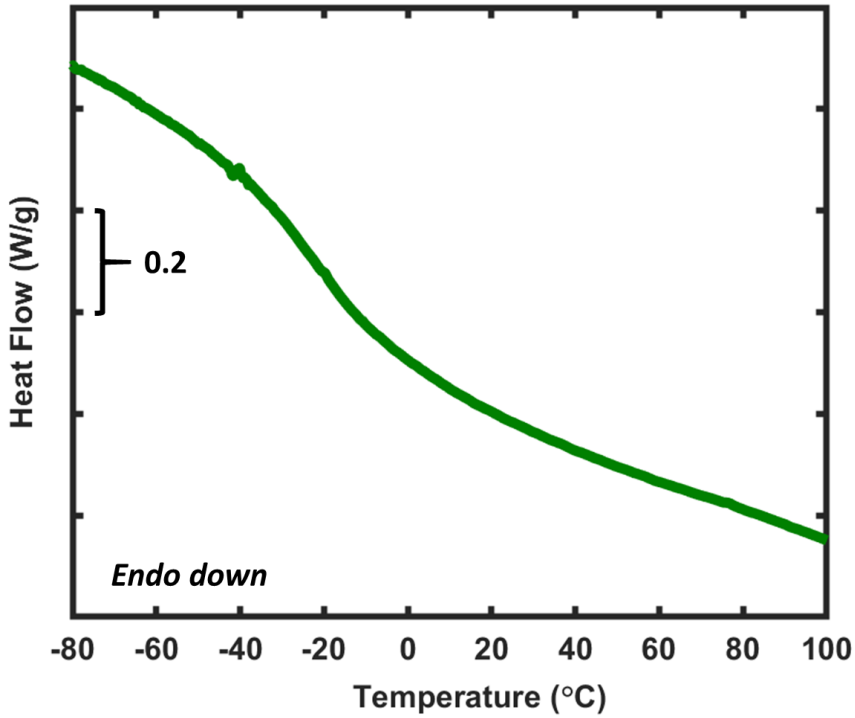

Figure S26. DSC thermogram (second heating, 10 °C/min) for **poly(4)**.

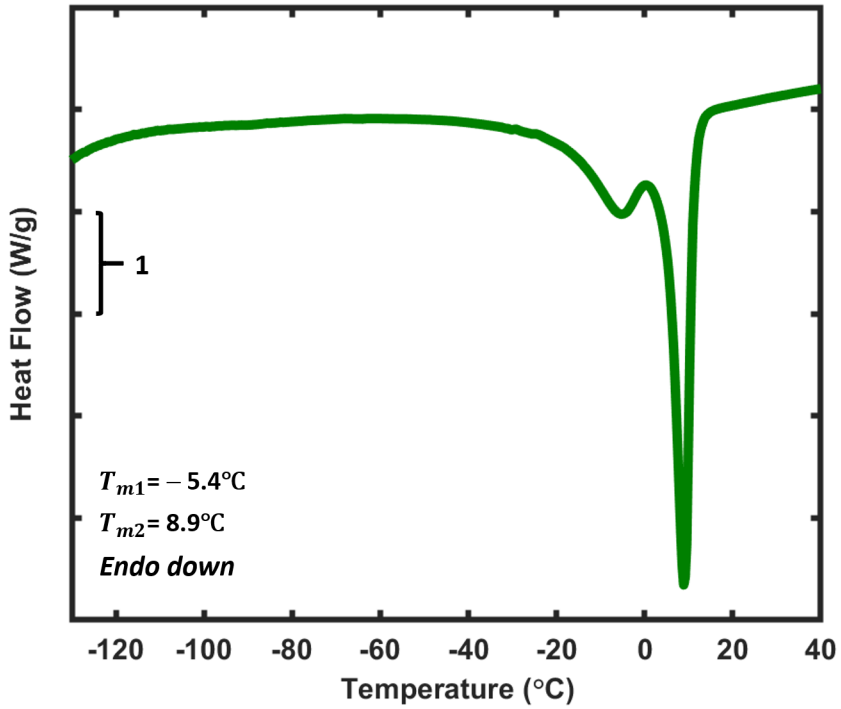

Figure S27. DSC thermogram (second heating, 20 °C/min) for **poly(5)**.

9. Copies of NMR

9.1 NMR spectrums of 2

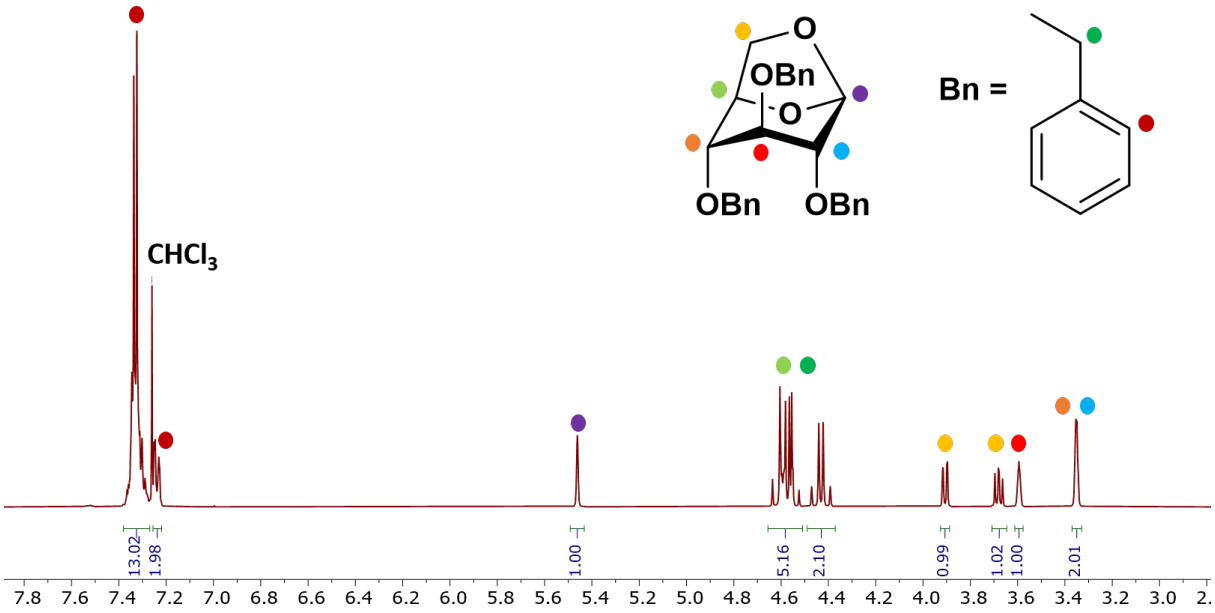

Figure S28. ^{1}H NMR spectra (400 MHz, $CDCl_3$) of monomer **2**.

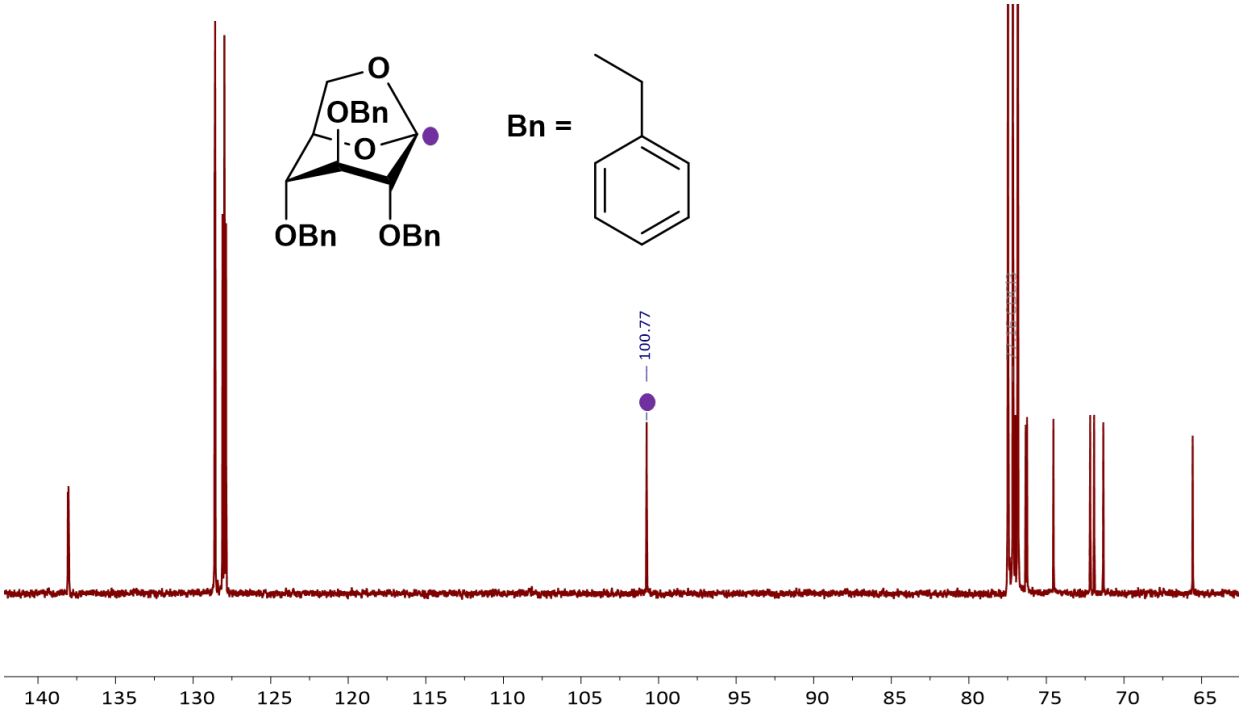

Figure S29. ^{13}C NMR spectra (100 MHz, $CDCl_3$) of monomer **2**.

9.2 NMR spectrums of 3

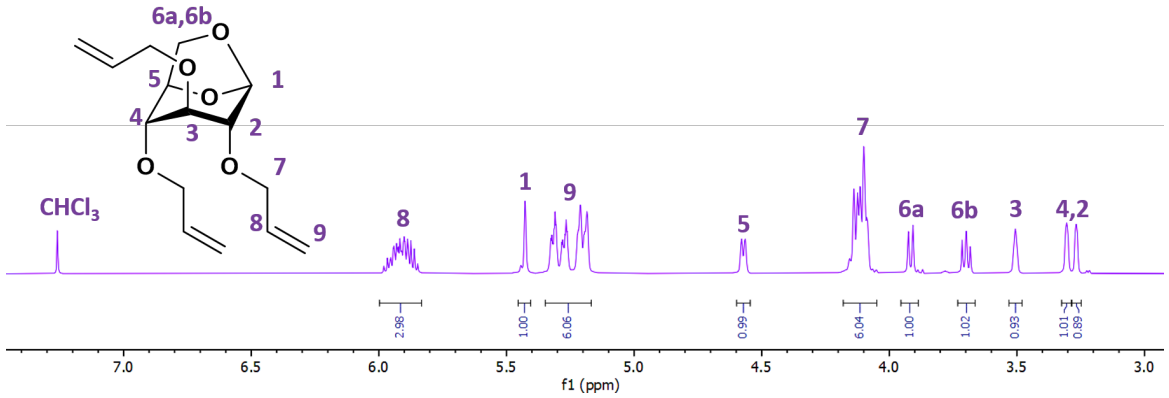

Figure S30. ^{1}H NMR spectra (400 MHz, $CDCl_3$) of monomer **3**.

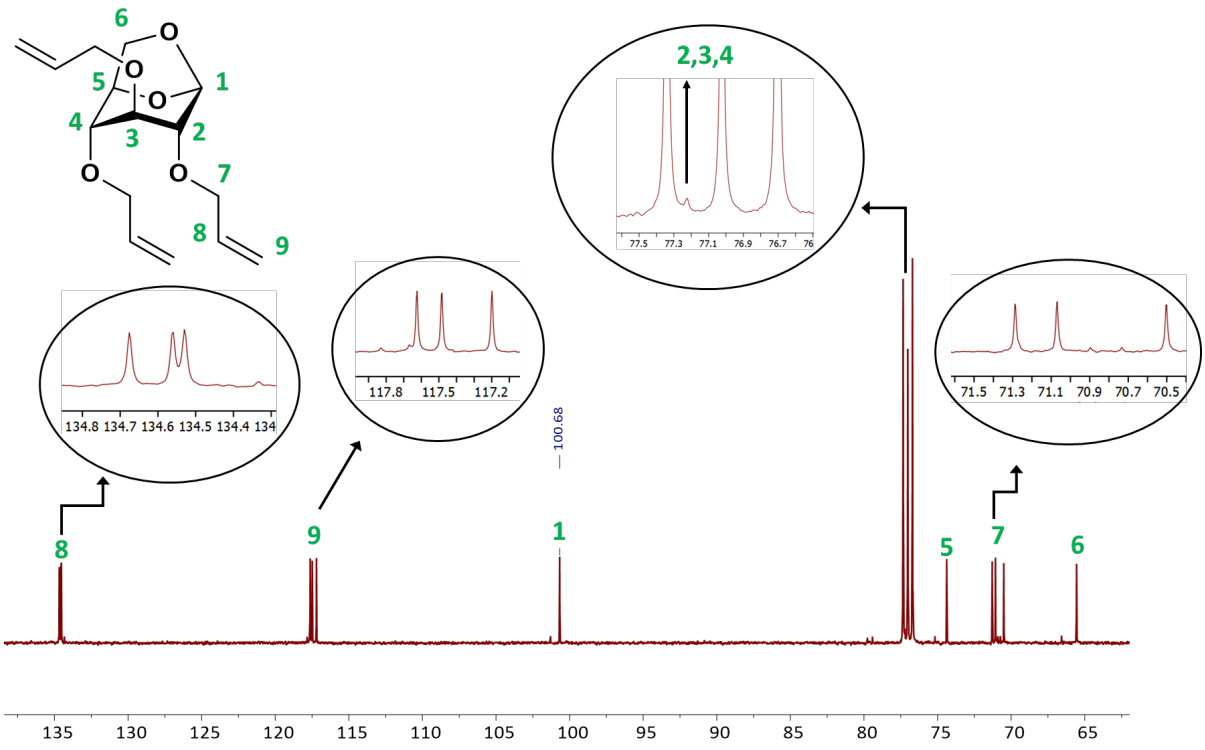

Figure S31. ^{13}C NMR spectra (100 MHz, $CDCl_3$) of monomer **3**.

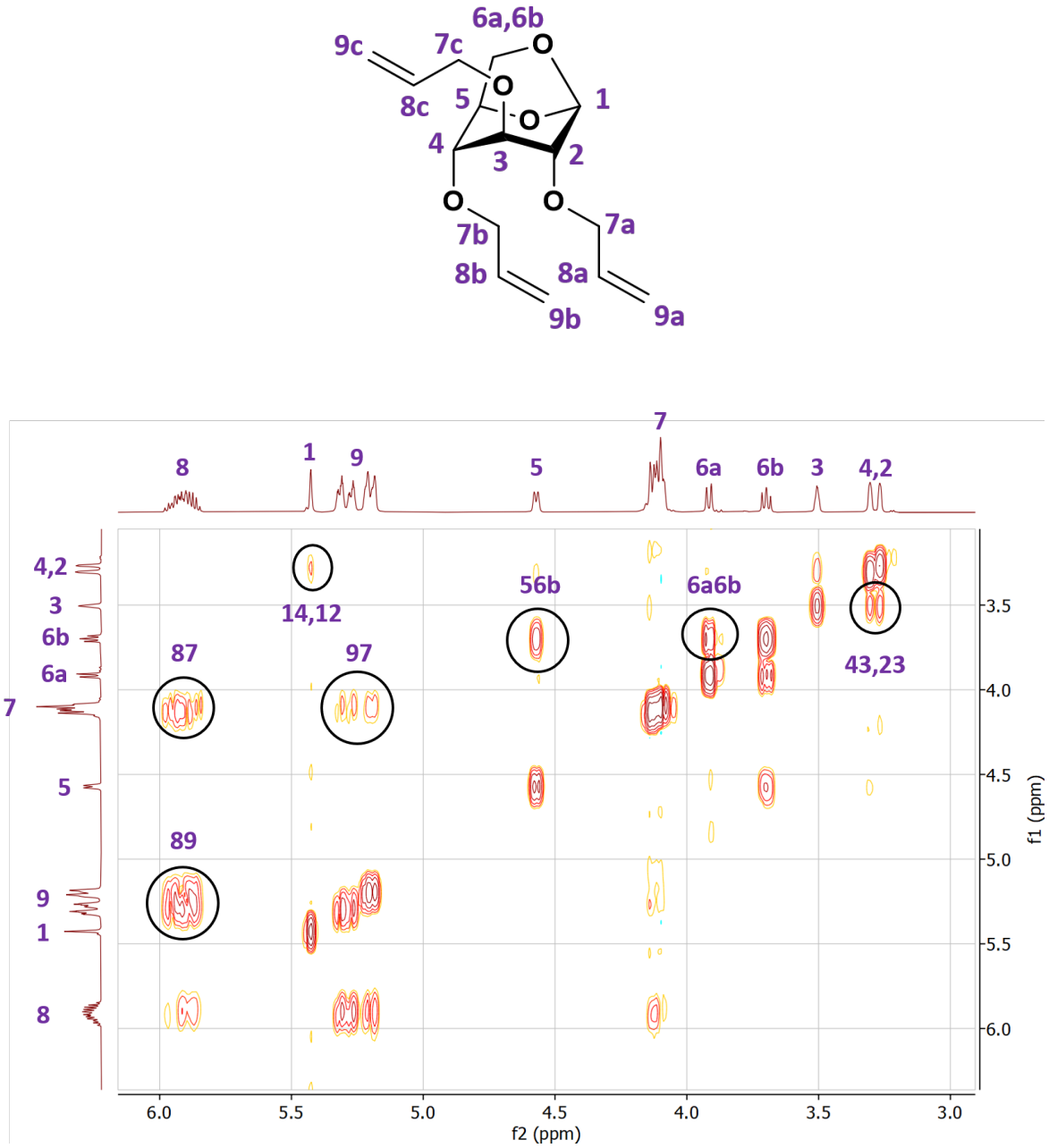

Figure S32. ^{1}H, ^{1}H COSY NMR Spectrum (400 MHz, $CDCl_3$) of monomer **3**.

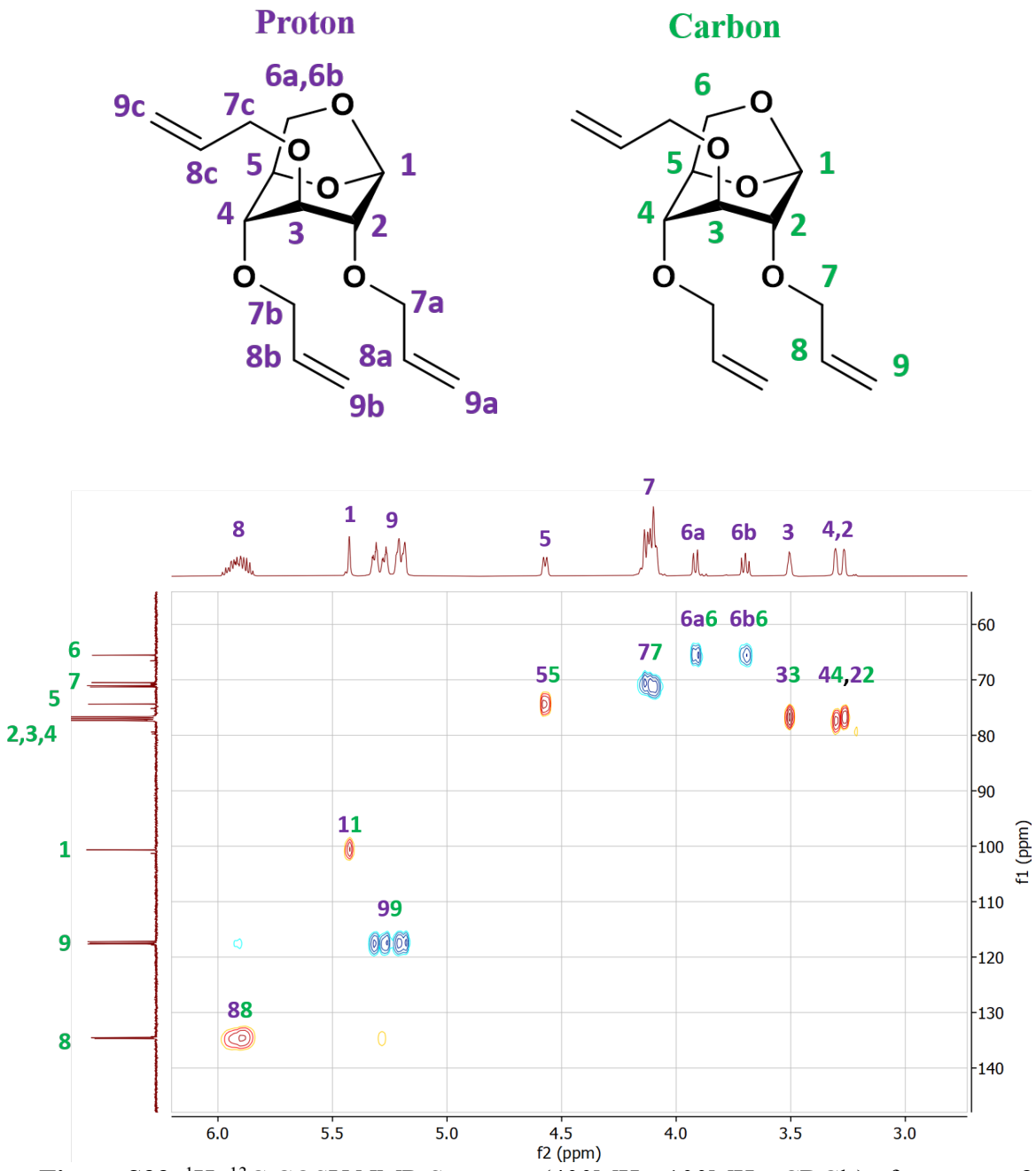

Figure S33. ^{1}H, ^{13}C COSY NMR Spectrum (400MHz, 100MHz, $CDCl_3$) of monomer **3**

(blue: negative phase, CH_2; red: positive phase, CH).

9.3 NMR spectrums of poly(2)

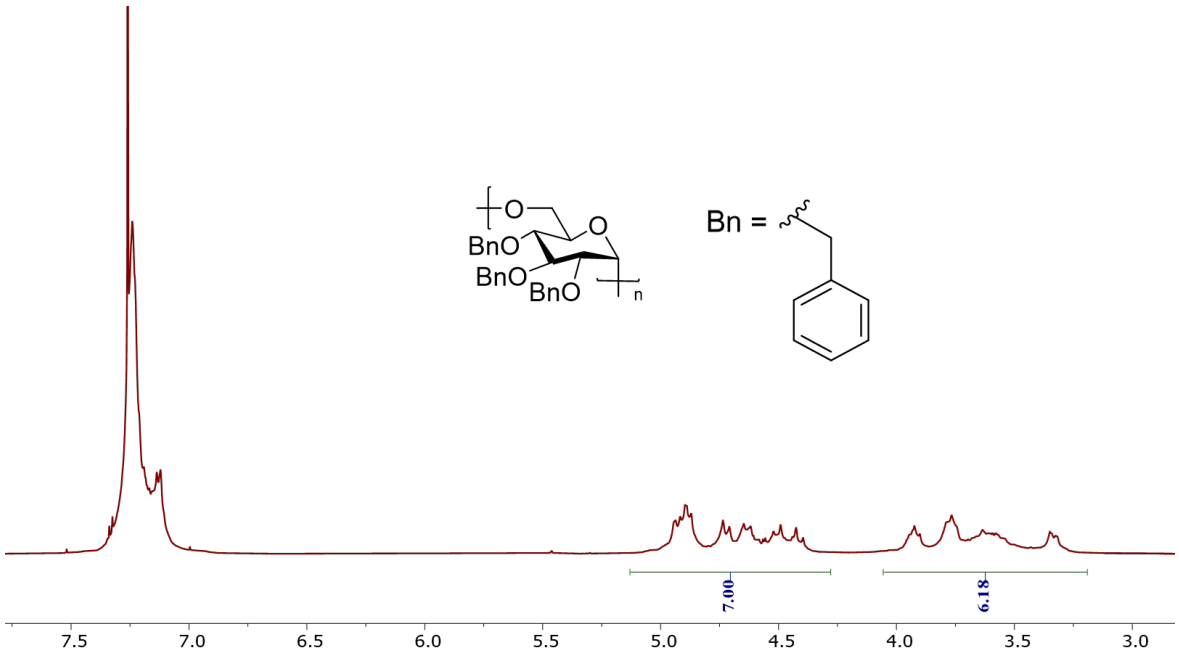

Figure S34. ^{1}H NMR spectra (400 MHz, $CDCl_3$) of **poly(2)**.

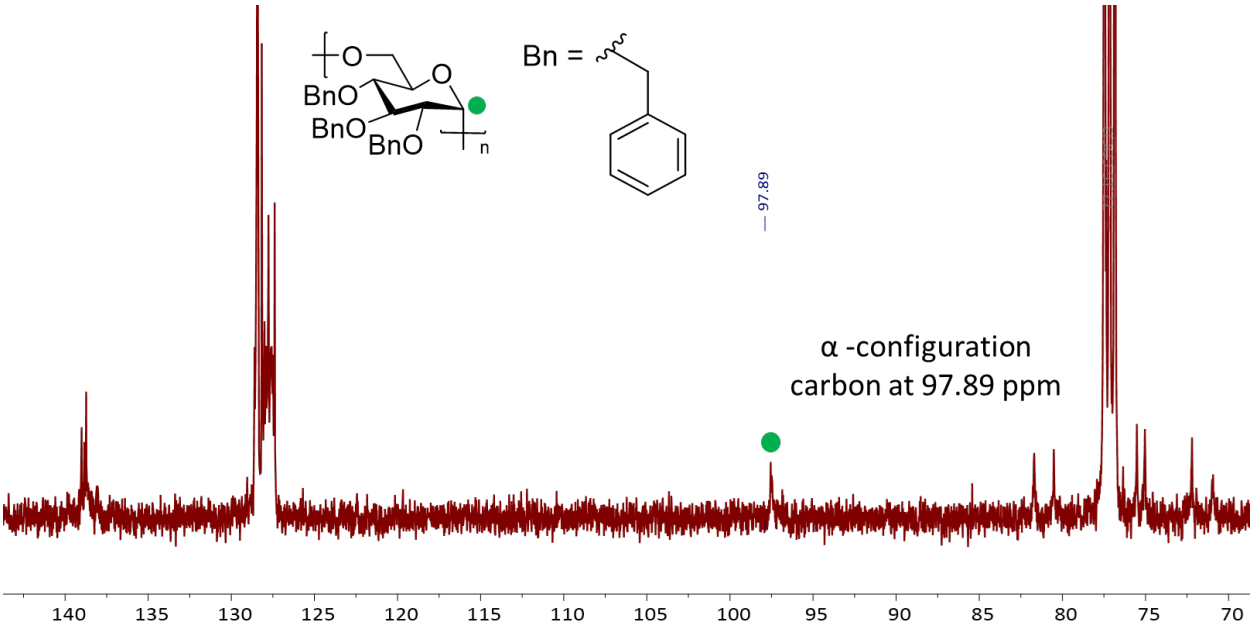

Figure S35. ^{13}C NMR spectra (100 MHz, $CDCl_3$) of **poly(2)**.

9.4 NMR spectrums of poly(3)

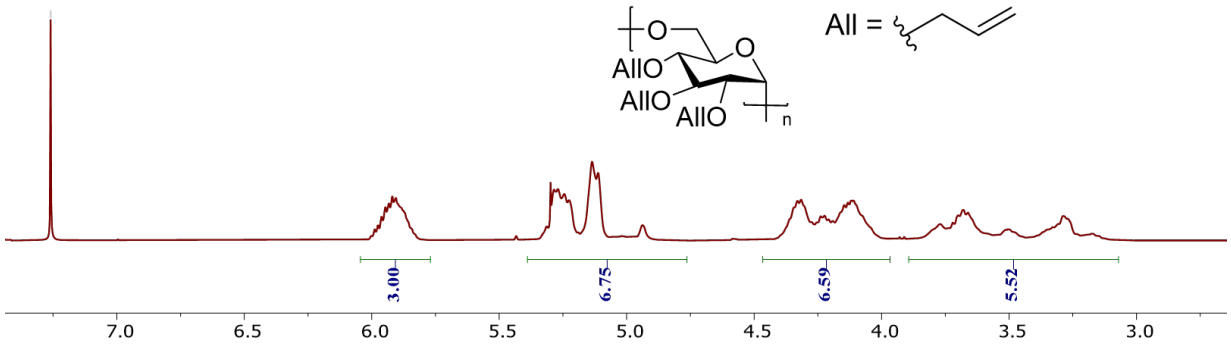

Figure S36. ^{1}H NMR spectra (400 MHz, $CDCl_3$) of **poly(3)**.

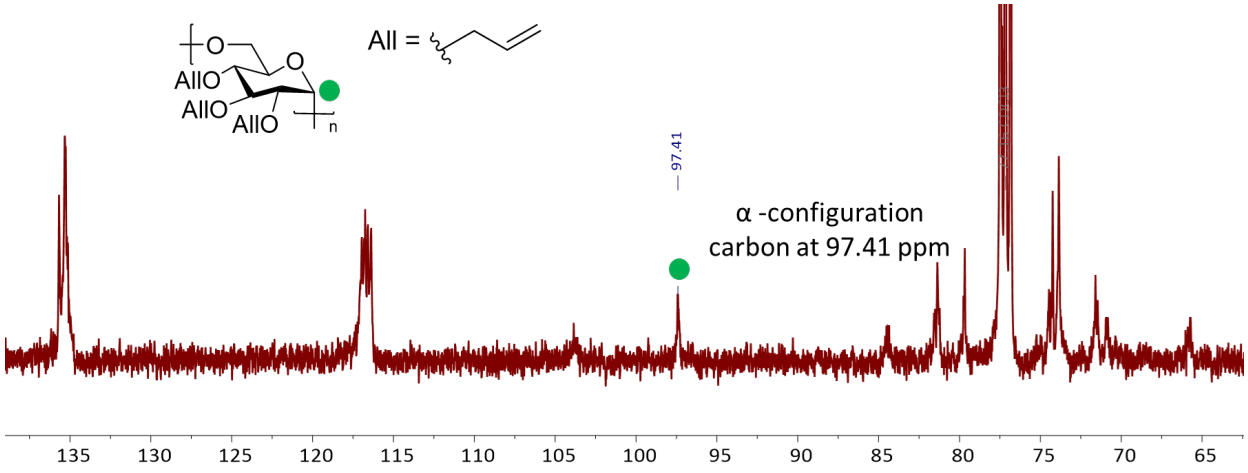

Figure S37. ^{13}C NMR spectra (100 MHz, $CDCl_3$) of **poly(3)**.

9.5 NMR spectrum of poly(4)

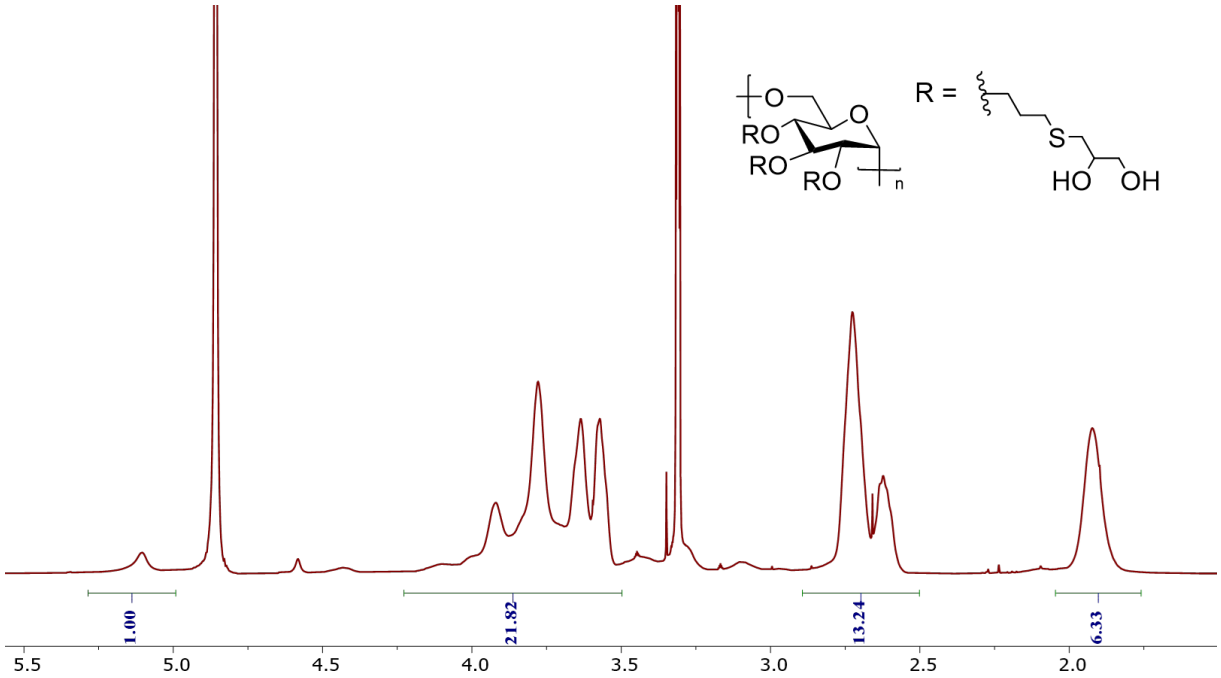

Figure S38. ^{1}H NMR spectra (500 MHz, CD_3OD) of **poly(4)**.

9.6 NMR spectrum of poly(5)

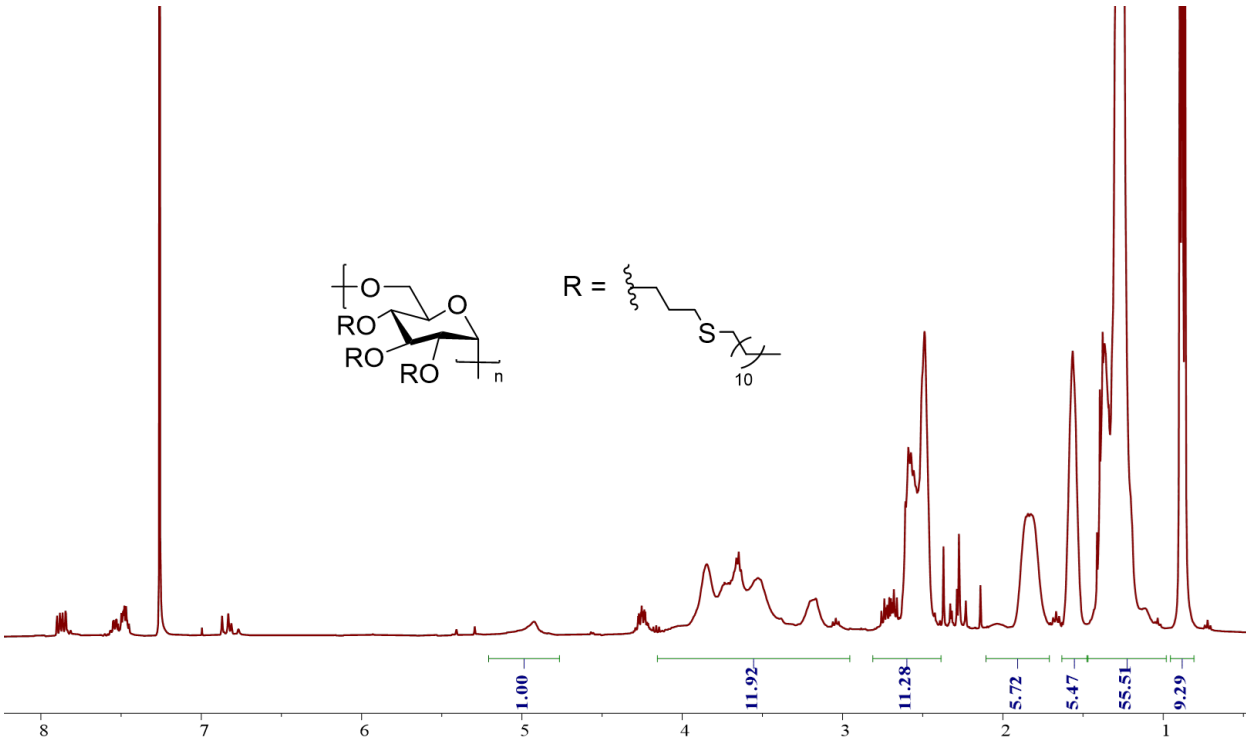

Figure S39. ^{1}H NMR spectra (400 MHz, $CDCl_3$) of **poly(5)**.

10. SEC Traces

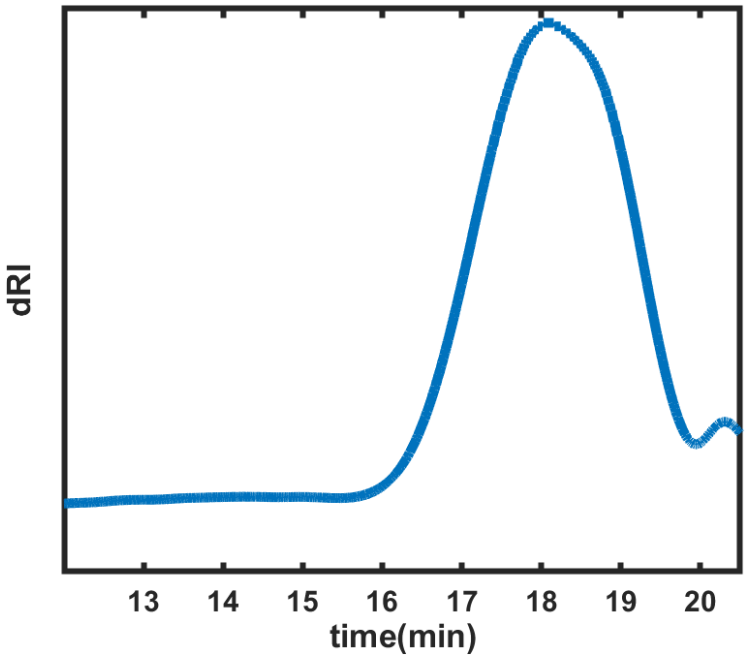

Figure S40. SEC trace of **poly(2)**.

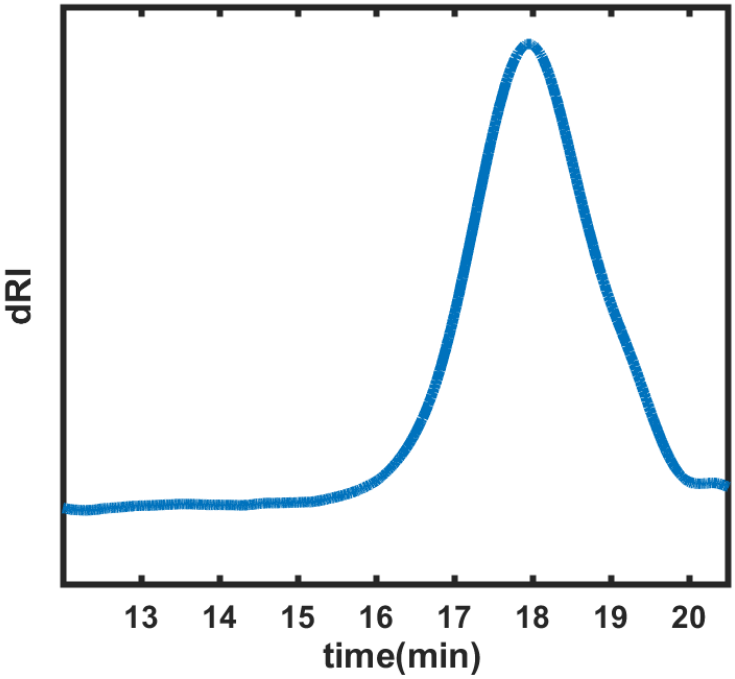

Figure S41. SEC trace of **poly(3)**.

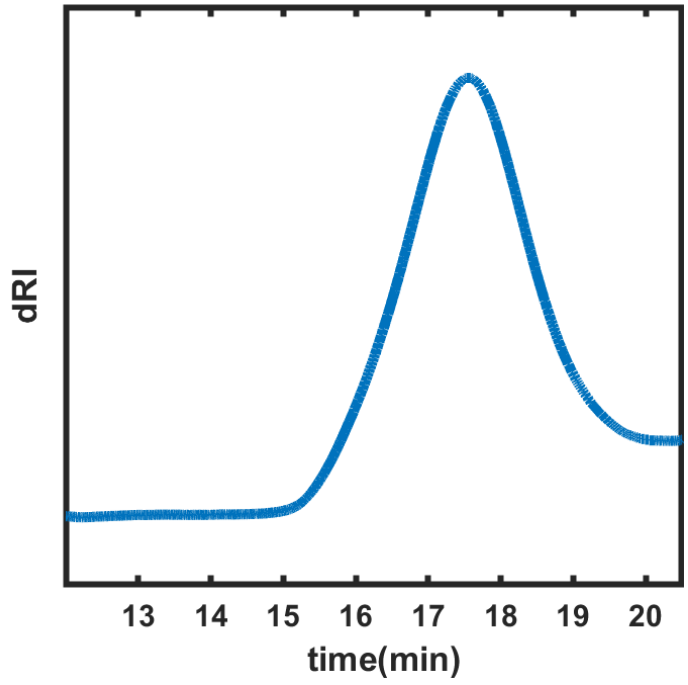

Figure S42. SEC trace of **poly(4)**.

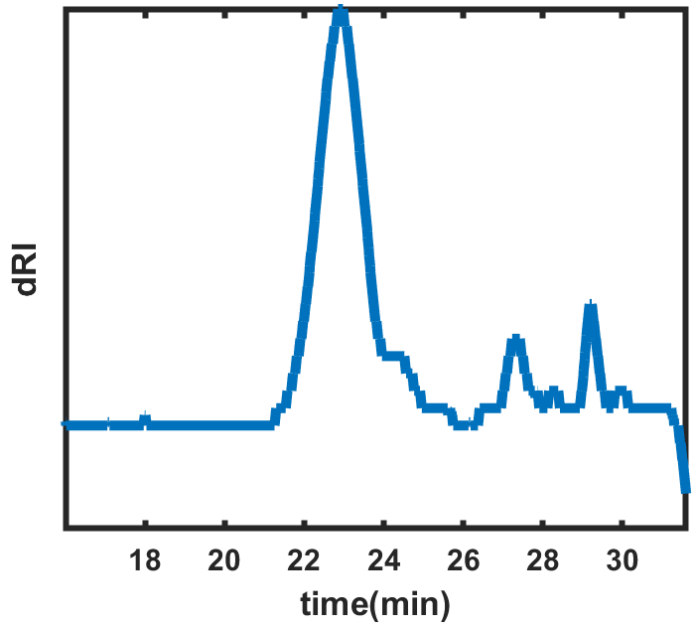

Figure S43. SEC trace of **poly(5)**.

11.Computational Methods

Extensive conformational analysis of reactants and products was carried out using procedures in the MacroModel package from Schrödinger[1] and the Merck Molecular Force Field (MMFF). Monte-Carlo Molecular Mechanics (MCMM) was employed with an extended torsional sampling.[2,3] Conformers within a range of 10 kcal mol^{-1} of the global minimum were considered for further analysis using Density Functional Theory (DFT). All DFT optimizations were carried out using the Gaussian16 electronic structure suite.[4] Following DFT optimizations were carried out at the M06-L/6-31+G(d,p) level in solvent phase using SMD solvation model[5], chosen to take advantage of the speed of the local functional. Here dichloromethane (DCM) solvent was used for the optimizations. Solvent single point calculations were further carried out for all conformers having electronic energies within a range of 5 kcal mol^{-1} to identify global minimum at the M06-2X[6] level of theory along with 6-311++G(d,p) basis set.

All reactants, products, intermediates, and transition-state structures (TSs) were optimized at the M06-L level of theory using LanL2DZ for Bi and the 6-31+G(d,p) basis set for all other atoms in the solvent phase using SMD solvation model. Experiments were performed in DCM solvent hence SMD is defined for DCM ($\varepsilon = 8.93$) was used for computations. To verify the nature of stationary points, as well as to compute vibrational partitions functions for use in free energy calculations, vibrational frequency computations were carried out at the same level of theory. TS structures were confirmed with one and only one imaginary frequency. Intrinsic Reaction Coordinate (IRC) calculations were carried out for the TS structures to confirm that they are connected to their respective reactants and products. Further solvent single point calculations were carried out using the SMD solvation model at the M06[6] and ωB97X-D[7] levels of theory along with def2-TZVP and SDD as a pseudo potential for Bi and def2-TZVP basis set for all other atoms. Gibbs free energies for all stationary points were obtained by adding the zero-point vibrational energy (ZPVE) and thermal energy corrections from standard statistical mechanics approximations at 298.15 K and 1 atm pressure, except that vibrational modes below 50 cm^{-1} were replaced with a value of exactly 50 cm^{-1} in vibrational partition function calculations. The binding free energies and Gibbs free energies of stationary points are discussed at the $SMD_{(DCM)}$/ωB97X-D/def2-TZVP, def2-TZVP|SDD(Bi)//$SMD_{(DCM)}$/M06-L/6-31+G(d,p), LanL2DZ(Bi) level of theory.

11.1 Coordination of Monomer 2 or 3 with Lewis Acid ($Bi(OTf)_3$ or $Sc(OTf)_3$)

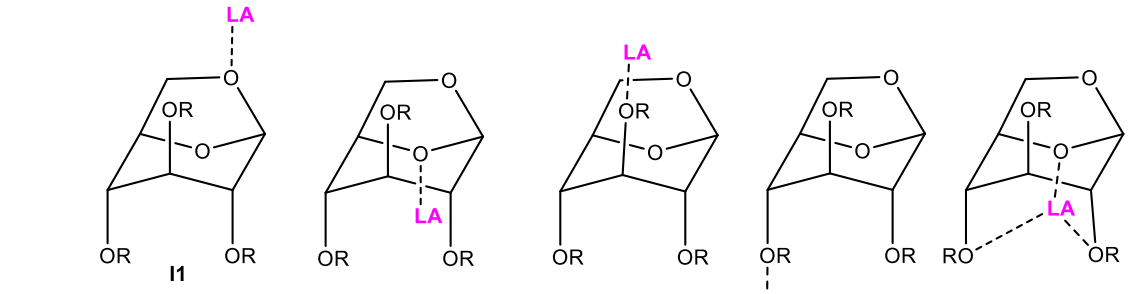

LA = $Sc(OTf)_3$					
R = All	-6.7	-3.6	-2.5	1.5	-19.6
R = Bn	-4.3	-7.3	-1.3	-1.0	-22.9
LA = $Bi(OTf)_3$					
R = All	-3.3	-1.7	-2.1	-0.1	-26.7
R = Bn	-2.8				
LA = PF_5					
R = All	4.6				
R = Bn	6.5				

Figure S44. Variety of coordination modes for monomer **2** or **3** to Lewis acids $Bi(OTf)_3$ or $Sc(OTf)_3$) and their corresponding binding free energies (in kcal/mol) are provided.

11.2 Optimized ring-opening transition state structures

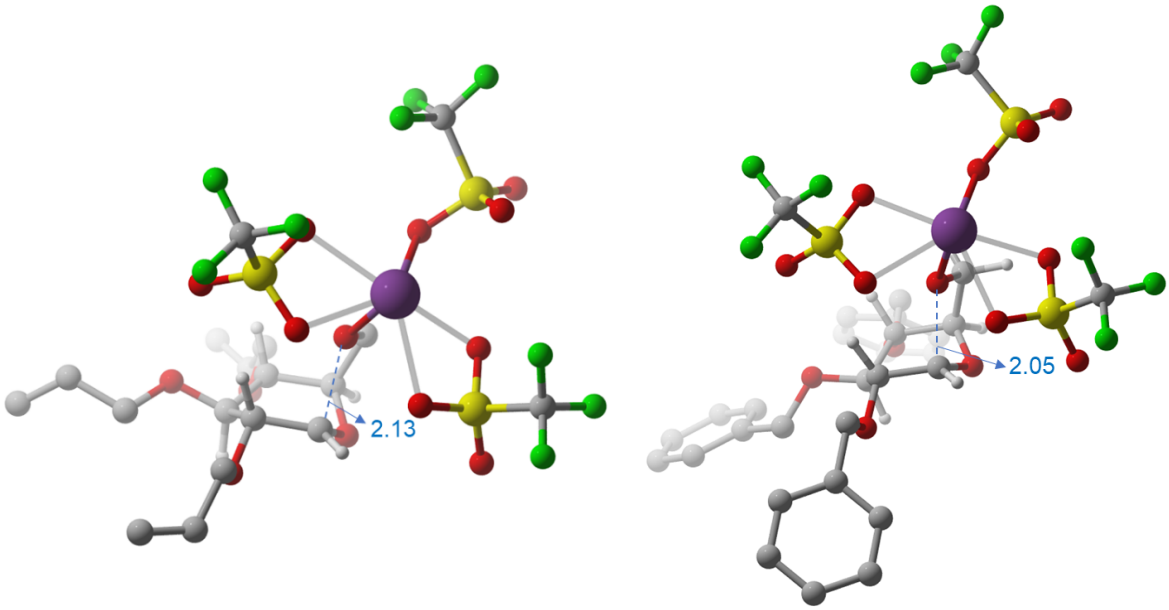

$TS1_{3\_Bi}$ (9.4)	**$TS1_{2\_Bi}$** (9.6)

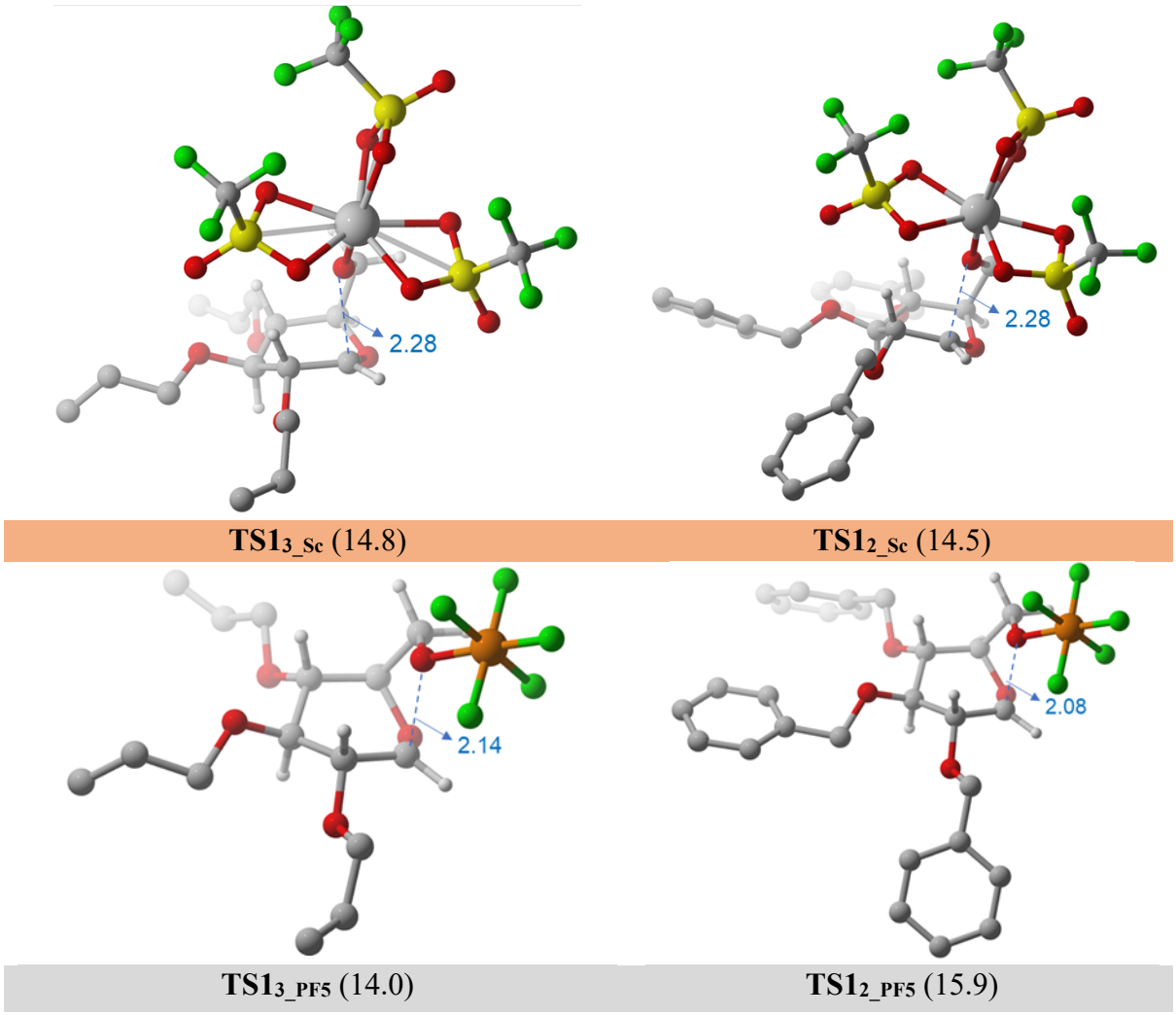

Figure S45. Optimized ring-opening transition state structures of allyl and benzyl substituted levoglucosan derivatives catalyzed by various Lewis acids ($Bi(OTf)_3$, $Sc(OTf)_3$ and PF_5) and their respective free energy of activations (kcal/mol) with respect to **I1** are provided in the parenthesis. Distances are in Å.

11.3 Nucleophilic Addition of Monomer to I2

The carbenium intermediate **I2**, is formed after the ring opening of allyl or benzyl derivatives of levoglucosan step. Subsequently, The nucleophilic addition of another monomer to the carbenium intermediate generates new C-O linkage through TS structure **TS2**. The nucleophilic addition step can occur either backside attack (**TS2α**) or frontside attack (**TS2β**) (Figure S46). We have considered a variety of conformations for this nucleophilic addition (**TS2α** and **TS2β**) step using $Bi(OTf)_3$ for allyl and benzyl monomers (Figure S47). Interestingly, the computed energetics evident that the formation of intermediate **I3** (1,6-α linkage) through **TS2α** is preferred over **I4** through **TS2β** (1,6-β linkage).

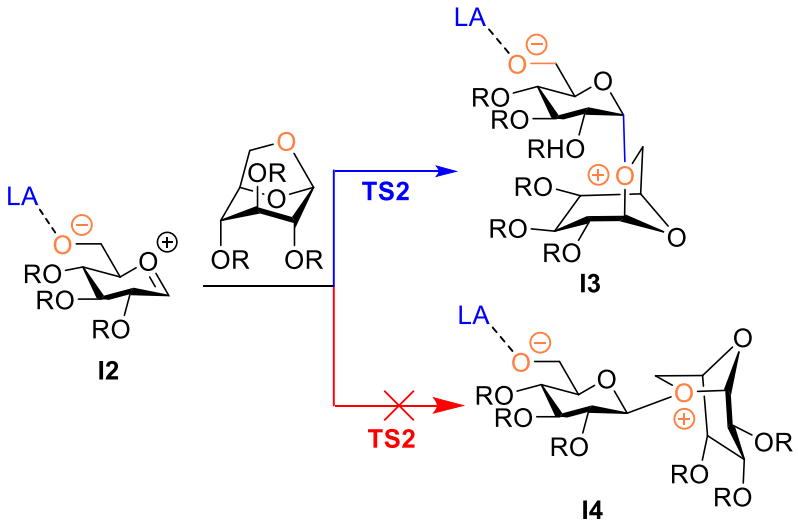

Figure S46. Nucleophilic addition of monomer to carbenium intermediate **I2** through transition state structures, **TS2α** and **TS2β**.

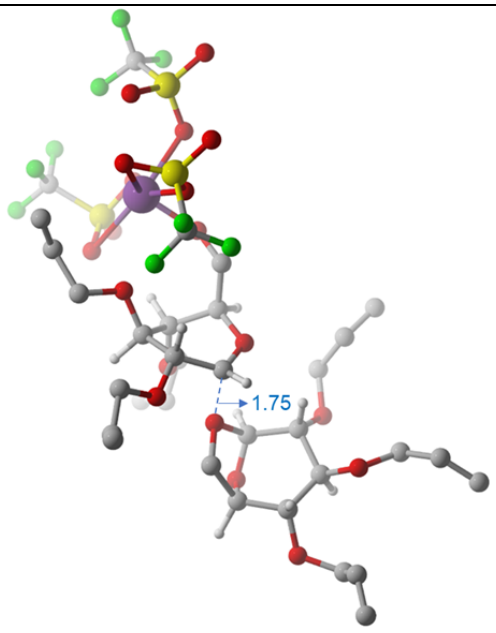	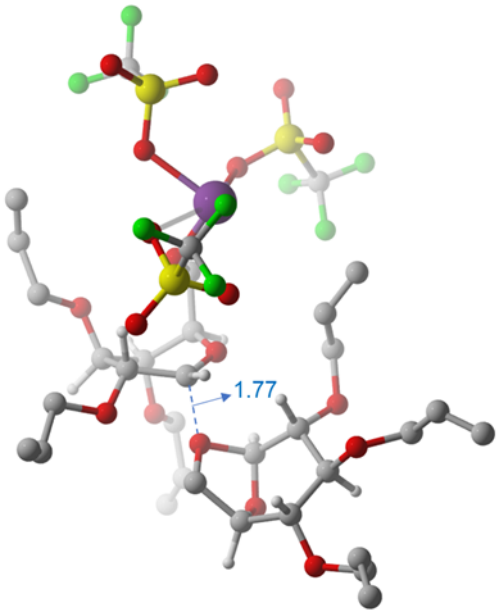
TS2$_{3_Bi_\alpha}$ (21.4)	**TS2$_{3_Bi_\alpha1}$** (28.5)

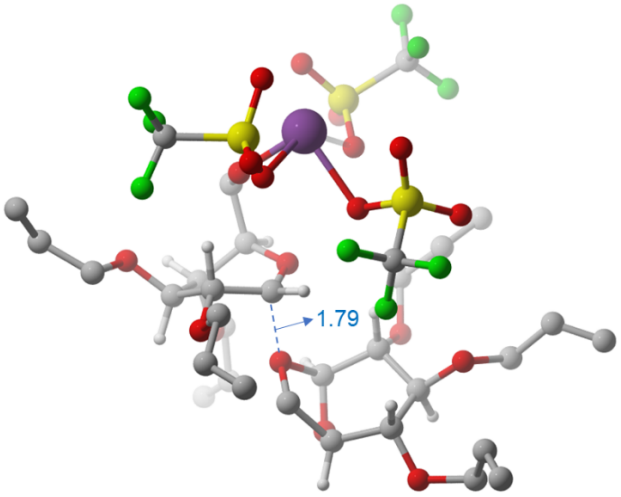	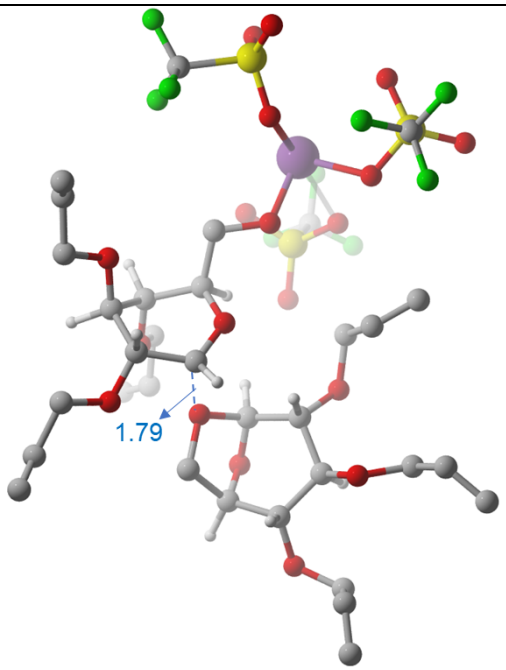
TS2$_{3\_Bi\_\alpha2}$ (23.6)	**TS2**$_{3\_Bi\_\alpha3}$ (27.0)
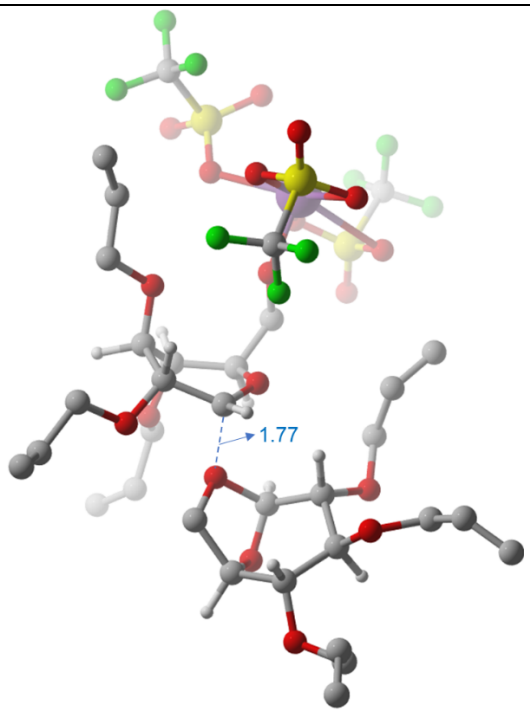	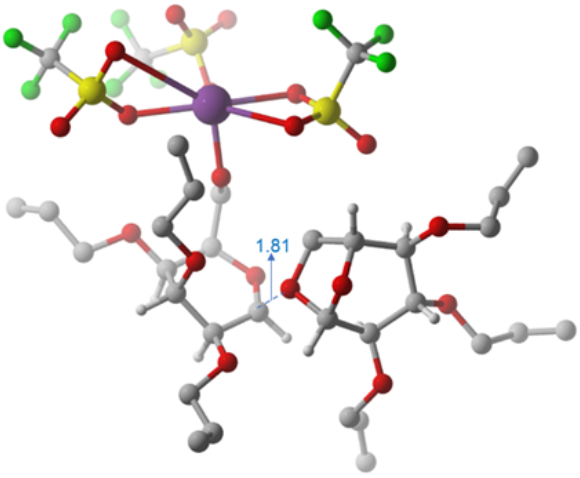
TS2$_{3\_Bi\_\alpha4}$ (30.1)	**TS2**$_{3\_Bi\_\beta}$ (25.4)

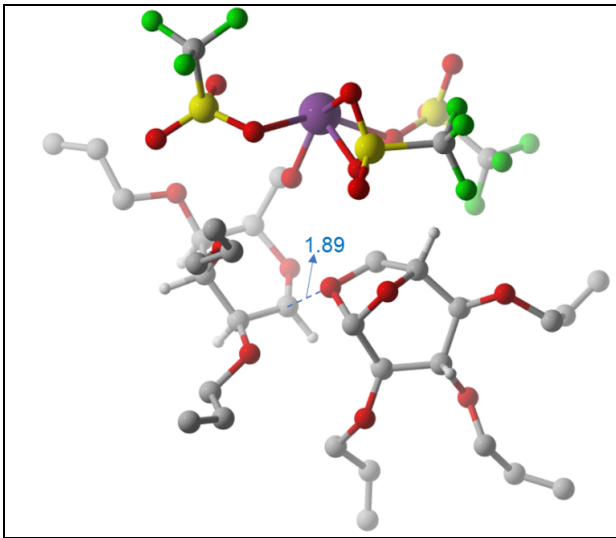	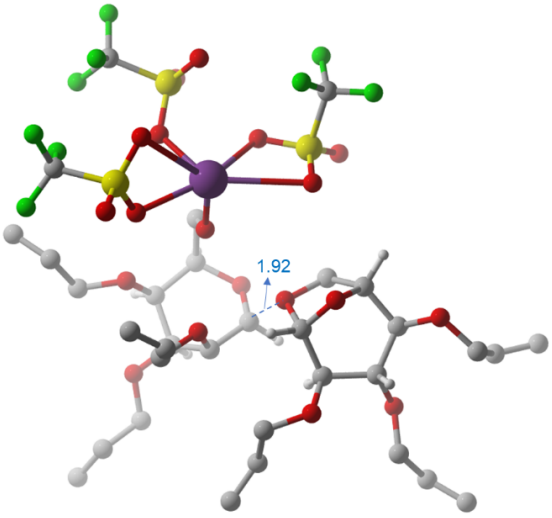
TS2$_{3_Bi_\beta1}$ (32.4)	**TS2$_{3_Bi_\beta2}$** (39.3)
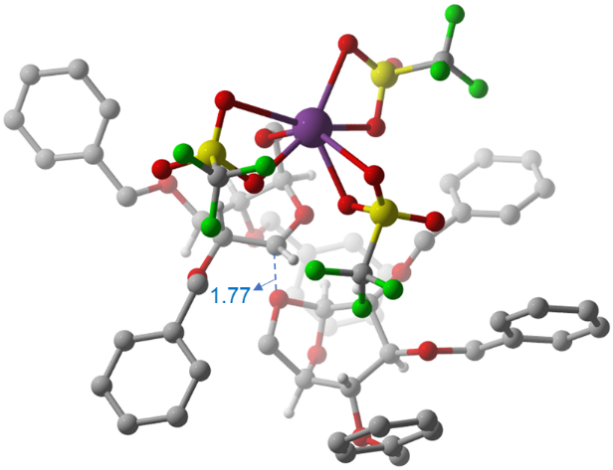	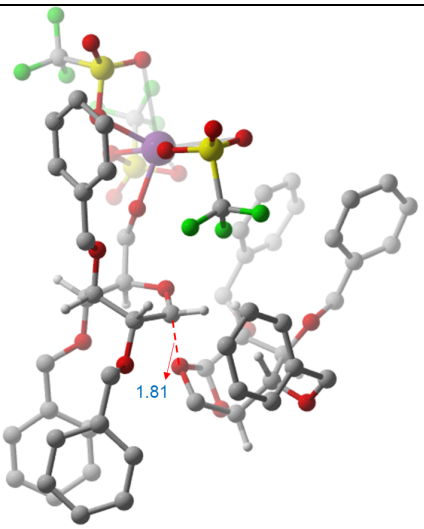
TS2$_{2_Bi_\alpha}$ (21.9)	**TS2$_{2_Bi_\alpha1}$** (40.6)
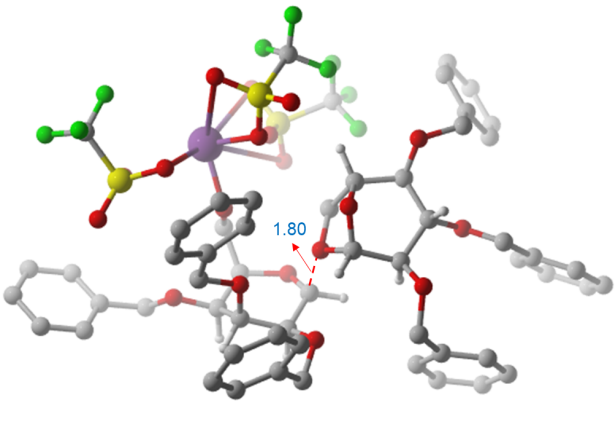	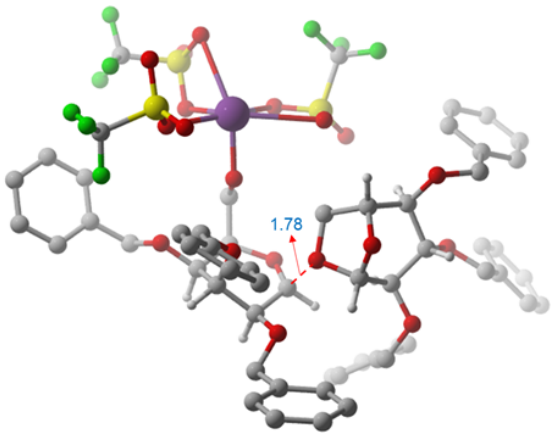
TS2$_{2_Bi_\beta}$ (30.6)	**TS2$_{2_Bi_\beta1}$** (34.9)

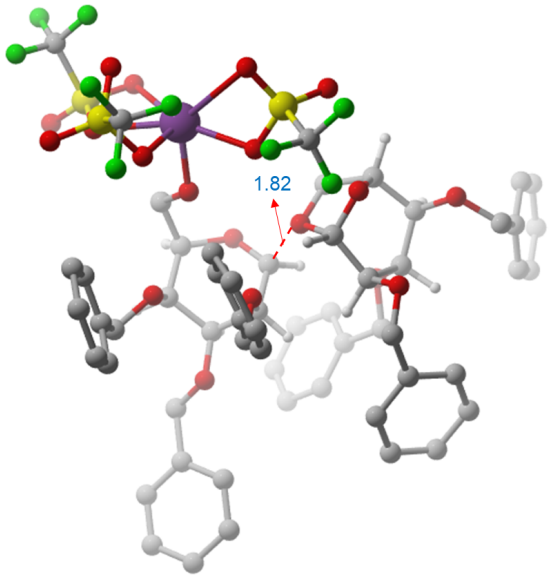	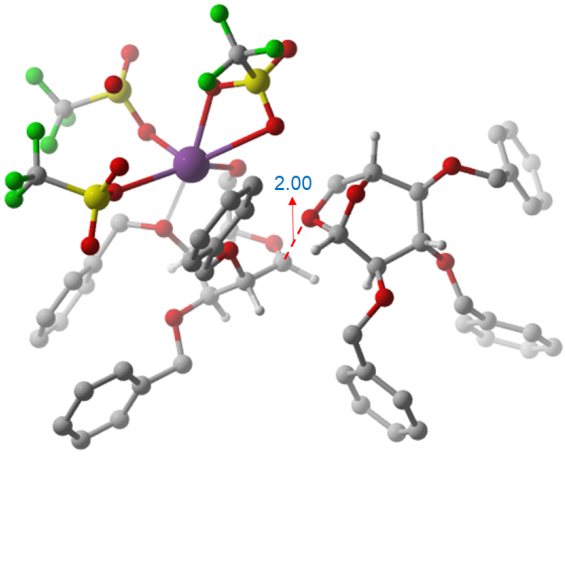
TS2$_{2\_Bi\_\beta2}$ (36.9)	**TS2**$_{2\_Bi\_\beta3}$ (33.0)
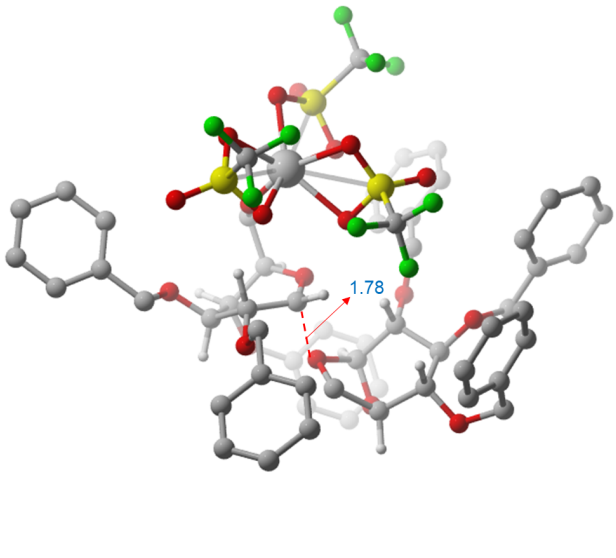	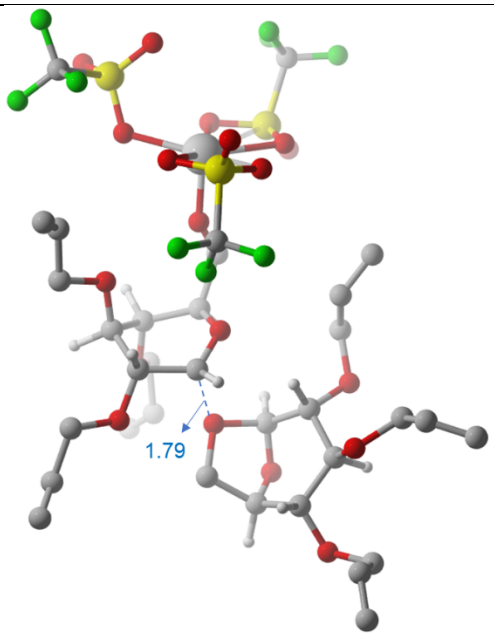
TS2$_{2\_Sc\_\alpha}$ (23.7)	**TS2**$_{3\_Sc\_\alpha}$ (23.6)

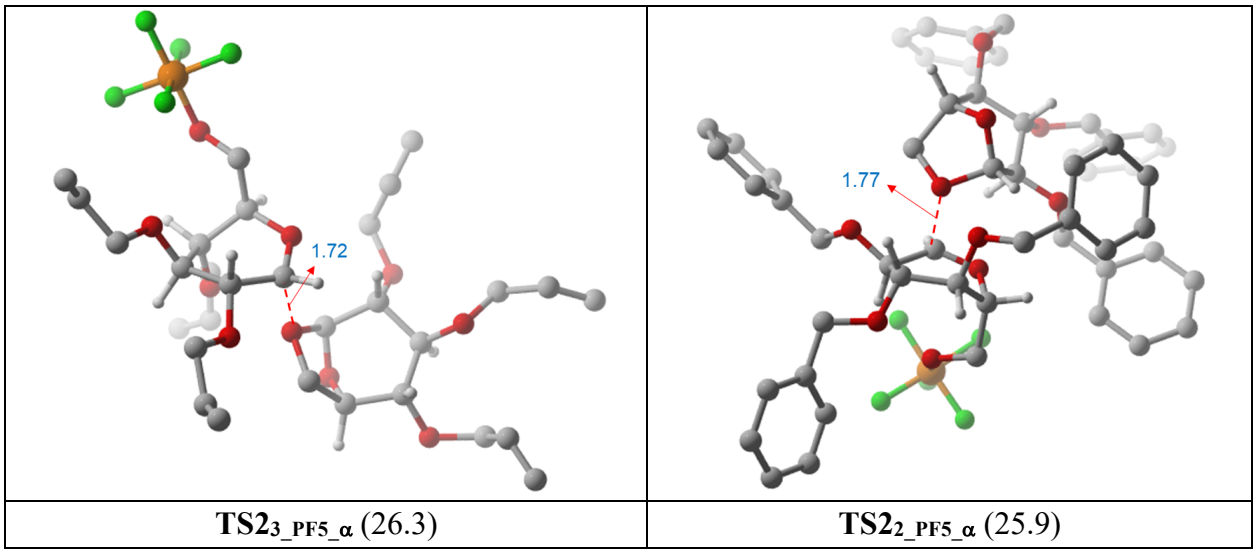

TS2$_{3\_PF5\_\alpha}$ (26.3)	**TS2**$_{2\_PF5\_\alpha}$ (25.9)

Figure S47. Possible optimized conformational transition state structures for the nucleophilic addition of monomer (**2**/**3**) to carbenium carbon of **I2** catalyzed by Lewis acids ($Bi(OTf)_3$ or $Sc(OTf)_3$ or PF_5). The free energy (kcal/mol) of activations with respect to **I1** are provided in parenthesis. Distances are in Å.

11.4 Alternative Pathways

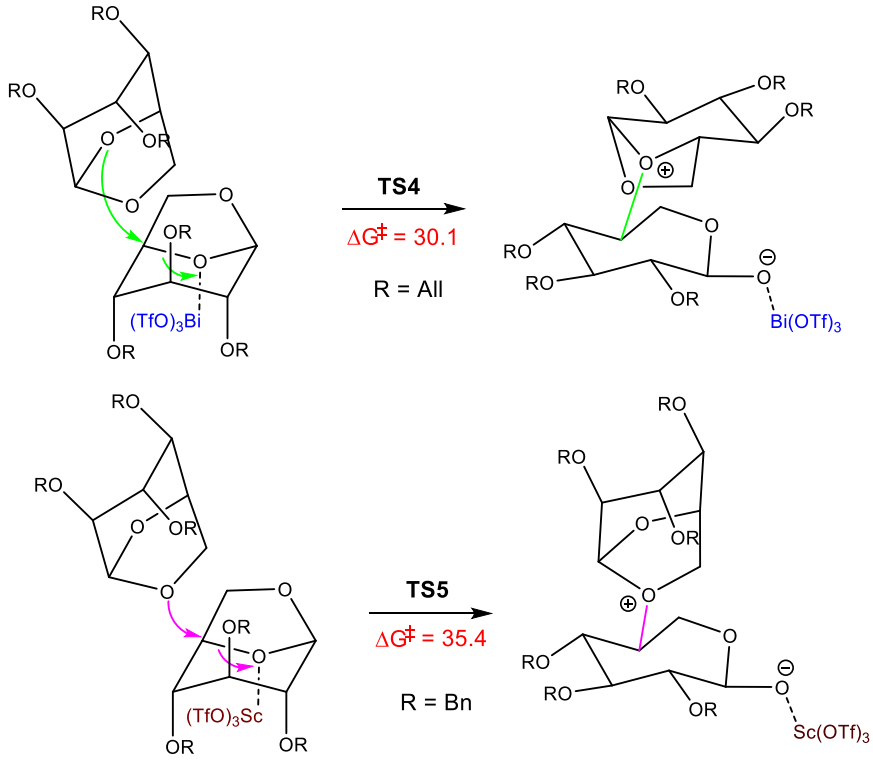

Figure S48. Alternative Possible Pathways for the cationic ring-opening polymerization of Levoglucosan derivatives catalyzed by Lewis acids. The free energy of activations ($\Delta G^{\ddagger}$ in kcal/mol) with respect to **I1** are provided.

12. References

1) H. Hu, J. You, W. Gan, J. Zhou and L. Zhang, Synthesis of allyl cellulose in NaOH/urea aqueous solutions and its thiol-ene click reactions, Polym. Chem., 2015, **6**, 3543–3548.
2) 1 C. J. Luo, E. Stride and M. Edirisinghe, Mapping the influence of solubility and dielectric constant on electrospinning polycaprolactone solutions, Macromolecules, 2012, **45**, 4669–4680.
3) M. Tobiszewski, J. Namieśnik, F. Pena-Pereira, Environmental Risk-Based Ranking of Solvents Using the Combination of a Multimedia Model and Multi-Criteria Decision Analysis. Green Chem. 2017, **19** (4), 1034–1042.
4) F. G. Calvo-Flores, M. J. Monteagudo-Arrebola, J. A. Dobado, J. Isac-García, Green and Bio-Based Solvents. Top. Curr. Chem. 2018, **376** (3), 1–40.
5) Macromodel: Schrödinger Release 2018−4: MacroModel; Schrödinger: LLC, New York, NY, 2018.
6) T.A. Halgren Merck molecular force field. I. Basis, form, scope, parameterization, and performance of MMFF94. J. Comput. Chem. 1996, **17**, 490−519.
7) T.A. Halgren. and R. B. Nachbar Merck molecular force field. IV. conformational energies and geometries for MMFF94. J. Comput. Chem. 1996, **17**, 587−615.
8) M. J. Frisch, G. W. Trucks, H. B. Schlegel, G. E. Scuseria, M. A.Robb, J. R. Cheeseman, G .Scalmani, V. Barone, G. A. Petersson, H. Nakatsuji, X. Li, M. Caricato, A. V. Marenich, J. Bloino, B. G. Janesko, R. Gomperts, B. Mennucci, H. P. Hratchian, J. V. Ortiz, A. F. Izmaylov, J. L. Sonnenberg, D. Williams-Young, F. Ding, F. Lipparini, F. Egidi, J. Goings, B. Peng, A. Petrone, T. Henderson, D. Ranasinghe, V. G. Zakrzewski, J. Gao, N. Rega, G. Zheng, W. Liang, M. Hada, M. Ehara, K. Toyota, R. Fukuda, J. Hasegawa, M. Ishida, T. Nakajima, Y.

Honda, O. Kitao, H. Nakai, T. Vreven, K. Throssell, J. A. Jr. Montgomery, J. E.Peralta, F. Ogliaro, M. J. Bearpark, J. J. Heyd, E. N. Brothers, K. N. Kudin, V. N. Staroverov, T. A. Keith, R. Kobayashi, J. NormandK. Raghavachari, A. P. Rendell, J. C. Burant, S. S. Iyengar, J. Tomasi, M. Cossi, J. M. Millam, M. Klene, C. Adamo, R. Cammi, J. W. Ochterski, R. L. Martin, K. Morokuma, O. Farkas, J. B. Foresman, D. J. Fox,Gaussian 16, Revision C.01, Gaussian, Inc., Wallingford CT, 2016.

9) A. V. Marenich, C. J. Cramer and D. G.Truhlar, Universal solvation model based on solute electron density and a continuum model of the solvent defined by the bulk dielectric constant and atomic surface tensions. J. Phys. Chem. B 2009, **113**, 6378−6396.

10) Y. Zhao and D. G. Truhlar, The M06 suite of density functionals for main group thermochemistry, thermochemical kinetics, noncovalent interactions, excited states, and transition elements: two new functionals and systematic testing of four M06-class functionals and 12 other functionals. Theor. Chem. Acc. 2008, **120**, 215−241.

11) J. D. Chai and M.Head-Gordon, Long-range corrected hybrid density functionals with damped atom-atom dispersion corrections. Phys. Chem. Chem. Phys., 2008, **10**, 6615-6620.